Datum
2024-09-09

Dnr
2021-200540

Projektnr
P2021-00283

Energimyndighetens titel på projektet – svenska	
Passagerarfärjor med helelektriska drivsystem – dimensionering, teknisk utvärdering och livscykelanalys vid drift i svenska farvatten	
Energimyndighetens titel på projektet – engelska	
Passenger ferries with fully electric drive systems – sizing, technical evaluation, and life cycle assessment for operation in Swedish waters	
Universitet/högskola/företag Chalmers Tekniska Högskola Aktiebolag	Avdelning/institution Electric Power Engineering (EPE) / Electrical Engineering
Adress 412 96 GÖTEBORG	
Namn på projektledare Emma Grunditz	
Namn på ev övriga projektdeltagare Chalmers division of Maritime Environmental Sciences (MES) and of Environmental System Analysis (ESA), as well as ABB and Berg Propulsion.	
Nyckelord: 5-7 st Drivsystem och batteri dimensionering, elektrisk framdrift, energiförbrukning, livscykelanalys, miljöutvärdering, passagerarfärja	

Preface

The project was finances by the Swedish Energy Agency, ABB and Berg Propulsion. The project has been carried out in collaboration between three departments at Chalmers; (1) Electrical Engineering, (2) Mechanics and Maritime Sciences and (3) Technology, Management and Economics, and with two industrial partners; Berg Propulsion and ABB. The industrial partners have acted as reference group and contributed with data and knowledge. In addition, discussions and data from Styrsöbolaget and Volvo Penta has also contributed to the project.

Table of contents

Sammanfattning

Det finns flera olika alternativa lösningar för en fossilfri sjöfart. För när- och kustsjöfart är batterielektrisk framdrivning mycket lovande. Syftet med denna studie var därför att utgå från en idag förbränningsmotordriven passagerarfärja som trafikerar svenska vatten, teoretiskt konvertera till batterielektrisk framdrift, samt att genomföra en livscykelanalys som jämför deras respektive miljöbelastning. För studien valdes passagerarfärjan Vesta som drivs av Styrsöbolaget och trafikerar fastlandet och öarna i Göteborgs södra skärgård, samt på Göta älv. Studien resulterade i dimensioneringen av en helt elektrisk drivlina inklusive batteri. Elmotorer med och utan magnet studerades, samt växelriktare och batteri med två olika kemi vilka optimerades mot hög energi respektive hög effekt. Material och energiåtgång för de olika komponenterna i drivlinan uppskattades och kopplades till en livscykelanalysmodell. Laddinfrastrukturen och de återstående delarna av fartyget inkluderades också i modellen, men på ett mer allmänt sätt. Därefter sammanställdes alla delar till en miljöpåverkansbedömning avseende global uppvärmning, lokala utsläpp och resursanvändning. Alla undersökta batterielektriska färjealternativ visade sig minska den globala uppvärmningspotentialen med mer än 90 % jämfört med en motsvarande dieselelektrisk färja som använder marin gasolja.

Summary

The shipping sector is in a transition to be fossil free and there are several different alternative solutions. For short sea and costal shipping battery-electric propulsion is very promising. The aim of this study was therefore to conduct a full life cycle assessment of a combustion propelled passenger ferry operating in Swedish waters, as well as of a retrofitted battery electric version of the ferry. A further aim was to examine the proportions of the environmental burden that falls on the battery, driveline components and the rest of the ship, as well as to compare the results with the diesel driven version. The study was based on the passenger ferry Vesta which operates by Styrsöbolaget between mainland and islands in Gothenburg's southern archipelago, as well as on the river Göta Älv. The project resulted in the dimensioning of a fully electric drivetrain including battery pack. Electric motors with and without magnets were studied, an inverter unit and batteries of two different chemistries, and optimized for energy respective power. Technical results were then linked to a life cycle assessment model where the data inventory analysis for the electric drivetrain and operation was the focus. The charging infrastructure and the remaining parts of the vessel were also included in the inventory model, however in a more general manner. Then all parts were compiled into an environmental impact assessment regarding global warming, local emissions and resource use. All battery-electric ferry options investigated was shown to lower the global warming potential with more than 90% compared to an equivalent diesel-electric ferry using MGO.

Introduction/Background

The United Nations (UN) body for international shipping, International Maritime Organization (IMO), has the goal of reaching zero emissions of greenhouse gas emissions from shipping around 2050 (MEPC, 2023). In the European Union (EU), shipping has been included in the European trading system for greenhouse gases emissions. In addition, Sweden has as a national goal to reduce the transport sector's emissions of greenhouse gases sharply in a relatively short time, to have no net emissions at all by 2045, and further in time to even have negative emissions. This ambitious goal requires work on several fronts within industry, society and academia, but also through collaborations between them.

To reduce shipping's climate impact, both a transition to fossil-free fuels and more efficient propulsion technologies are needed. One alternative could be electrification, provided that the electricity production is done with renewable sources. The suitability for electrification of different ship segments varies depending on its very different conditions. However, for coastal shipping and liner shipping, electrification is a possibility and today there are many examples of hybrid and fully electrified ships. Most of these operate in Europe and are car or passenger ferries and approximately 25% of these are fully electrified. An example is the all-electric Danish ferry Ellen, where the CO_2 emissions for its fixed route have been greatly reduced compared to the traditional ferries (Danfoss, 2022).

It is well known that electrification of ship propulsion can reduce energy consumption and direct emissions during operation, however, what is missing are studies that evaluate in detail the total environmental impact from a life cycle perspective and at the same time take the impact from the design of the ship's propulsion system into account.

The aim of this study was therefore to conduct a full life cycle assessment of a not yet electrified passenger ferry operating in Swedish waters, to examine the proportions of the environmental burden that falls on the battery, driveline components and the rest of the ship, as well as to compare the results with a diesel driven version.

Starting from a chosen diesel driven passenger ferry, Vesta, and its operating profile in Gothenburg’s southern archipelago, a fully electric drivetrain and battery pack were dimensioned in terms of power and energy requirement including estimation of effect on mass. Electric motors with and without magnets were studied, an inverter unit and batteries of two different chemistries, and optimized for energy respective power. To keep the battery size down, both opportunity and night charging were considered. Ship resistance, and load dependent drivetrain losses were modelled, whereupon the electric energy consumption from the grid was estimated. Technical results were then linked to a life cycle assessment model where the data inventory analysis for the electric drivetrain, battery and operation was the focus. The charging infrastructure and the remaining parts of the vessel were also included in the inventory model, however in a more general manner. Then all parts were compiled into an environmental impact assessment regarding global warming, local emissions and resource use.

The project was divided into the four main parts:

Part 1 - Determine case-ferry, drive line, battery and route

Part 2 - Electric motor, inverter and battery modelling

Part 3 - Quantification of propulsion energy and fuel consumption

Part 4 - Environmental assessment

Implementation and results

Here the methods and results of the four project parts are presented.

Part 1 - Determine case-ferry, drive line, battery and route

This section presents the methods used and part results regarding the ferry chosen as a base for the study, its current and retrofitted propulsion system, as well as an estimation of its required propulsion power as a function of operation.

The required mechanical output power from the propulsion motor is proportional to the ship's resistance and speed but inversely proportional to the combined efficiency of the drive system, hull and propeller. The estimation of these factors is described below.

Chosen case-ferry to study

During the first part of the project, various passenger ferries operating in Sweden, and preferably Gothenburg, were considered as possible candidates for the study. The target was to find a relatively small passenger ferry operating along a route which could be suitable for conversion to battery electric propulsion instead of today's diesel propulsion. As there were already examples of short distance hybrid electric ferries operating on the river of Göta älv in Gothenburg, a slightly longer route was targeted. Therefore, it was chosen to base the study on the passenger ferry Vesta which operates by Styrsöbolaget between mainland and islands in Gothenburg's southern archipelago, as well as on the river Göta Älv. Today Vesta is propelled by two diesel engines via a co-driving gear and a single controllable pitch propeller (Styrsöbolaget, 2023). Vesta's general ship specifications are presented in ***Table 1***, and component specifications in ***Table 2***. For the life cycle assessment (LCA) use-phase a part load condition was here determined as with 60% fuel in bunkers and 50% of passengers.

Table 1. Vesta's general ship specifications (Styrsöbolaget, 2023), (Styrsöbolaget, 2022),(Volvo Penta, 2021).

Number of passengers	447	
Top speed	13.5	knots
Overall length	34.4	m
Breadth at widest point	8.0	m
Draught at full load	2.39	m
Mass, light weight	212	ton
Mass, dead weight	65	ton
Mass, full load	277	ton
Mass, part load	254	ton

Table 2. Vesta's onboard equipment specifications (Styrsöbolaget, 2023), (Styrsöbolaget, 2022), (Volvo Penta, 2021),(Vesta, 2024).

Hull	Ice graded, steel hull
Main propulsion engines	2 x Volvo Penta D16 MH 600, each 441 kW, 3096 Nm, 1800 rpm, glycol cooled
Tanks, bunker, day	16 m^3, 0.5 m^3
Gear	Reduction ratio 1:4.84
Propulsion propeller	One controlled pitch propeller (CPP) with three blades, max. 372 rpm, hydraulic pitch control
Bow propeller	Hydraulic actuator
Auxiliary engine, generator	60 kW el.
Heat pump	3.8 kW el, 17.4 kW heat
Oil burner	155 kW heat

Chosen drive and energy system to study

It was decided that the electrified version should replace the propulsion diesel engines and bunkers with two sets of identical drive systems comprising one electric motor, one inverter and a battery energy storage, whereas the propeller and gear box should be kept, as could be anticipated in an actual retrofit conversion. The auxiliary diesel generator and oil burner were replaced by an inverter, higher-rated heat pump, and dc-dc converter for 12 V loads. The two versions of the case-study ferry are illustrated in *Figure 1*.

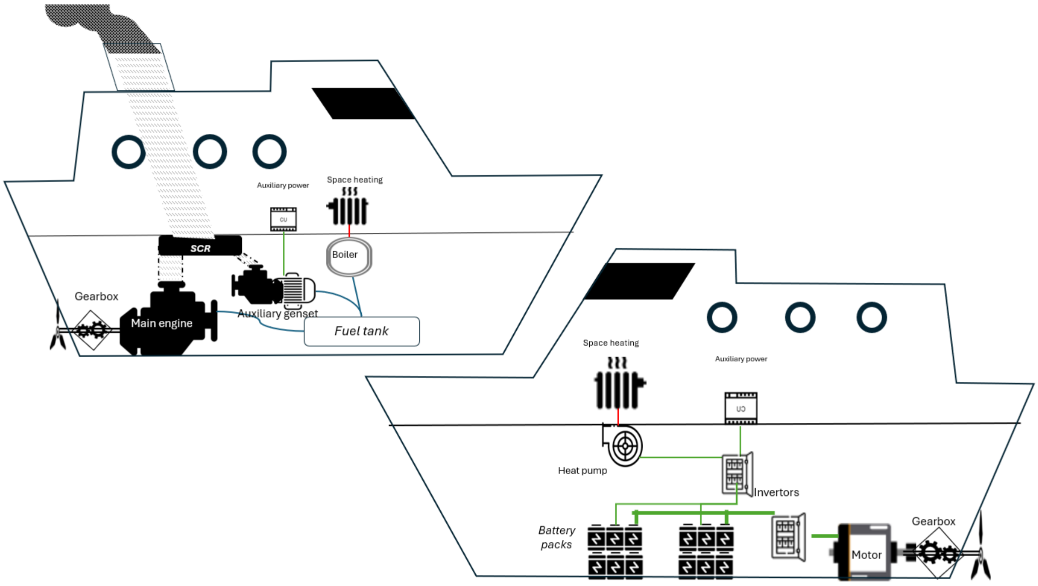

Figure 1. The case study ferry with a conventional (left) and battery-electric propulsion system (right).

The next target was to determine which technical variations in powertrain and battery storage to model and evaluate further in the project. As a basis for such decisions, specification data for around 30 existing fully electric ships of various sizes regarding manufacturer, owner, operational route, loading capability, dimensions, performance, as well as the drive system, battery and charging solution was collected and compiled in a project internal spreadsheet. The specification data of existing battery electric ferries

(BEFs) are presented in ***Table 12 - Table 15*** in the Appendix. The data was found in sources such as scientific publications, official reports, media and ship builder websites. The fleet of fully electric ferries was quite small, largely diverging for most specification parameters, and detailed data on the drive system, battery and charging components and configuration of the ferries was scarce.

As a complement, specification data from a dozen marine **battery** manufacturers was also collected regarding aspects such as cell type, voltage, charge and energy capacity, charge and discharge current/power and corresponding C-rate, cycle life, weight and volume on both cell and pack level. For positive electrode materials, data on batteries with Lithium Nickel Magnesium Cobolt (NMC) were found from seven manufacturers and Lithium Iron Phosphate (LFP) from four manufacturers. For negative electrode materials, graphite is used in the majority of applications. An alternative negative electrode material used is Lithium Titanate Oxide (LTO)[2] whose specifications are obtained from four manufacturers. In many cases, the data is only provided for battery pack size, and in a few cases also on cell level. Generally, the manufacturers provide scalable battery packs. The C-rate for continuous charging/discharging range can be found between 0.4-3C for NMC batteries, 0.7-4C for LFP batteries, and 0.6-6C for the LTO containing batteries.

Before 2012, the Nickle Cobalt Aluminum Oxide (NCA) was the predominant positive electrode material among various types of lithium-ion batteries (LIBs). However, NMC is the most preferred chemistry in the maritime industry, followed by LFP batteries (mostly in China and France) presently (Hoedemaker, 2023). Based on the production capacities planned and announced for LIB cells for all applications, 44% of global cell capacity will be Ni-based, predominantly NMC, and 26% for Fe-based cell chemistry, predominantly LFP (Hettesheimer et al., 2023). For negative electrode material, graphite is expected to remain widely used (Hettesheimer et al., 2023). In terms of safety, NMC and LFP are considered more suitable for marine applications (DNV GL AS Maritime. , 2020). Considering the above aspects and data availability, NMC and LFP with graphite negative electrodes are shortlisted for the analysis.

Possible **electric machine** types for marine propulsion are induction machines (IM), permanent magnet synchronous machines (PMSM), and synchronous reluctance machines (SRM). However, their respective market share could not be acquired, and all could be deemed equally plausible for our application. It was decided that the study should concentrate on the PMSM type and possibly also the SRM. By doing this, a detailed scalable life cycle inventory model of an automotive PMSM, developed at Chalmers, could be utilized for both motor types, with updated mass of materials.

For redundancy in marine applications, two independent battery packs must be placed in two separate compartments on board (DNV-GL, 2020). Thus, each battery pack supplies one electric drive line. As in electric vehicles, an onboard dc electric system was chosen, without dc/dc-converters, to regulate the dc-bus voltage to the inverters. Hence, the dc-bus voltage will vary with the electric load on and relative energy content in the batteries. The dc-bus was targeted up to around 1000 V. A lower rated dc/ac converter is expected to supply auxiliary and heating loads, and an even lower rated rectifier to supply equipment on the bridge. The system's line diagram is presented in ***Figure 2***.

[2] LTO refers to the material for the negative electrode and is often combined with an NMC positive electrode.

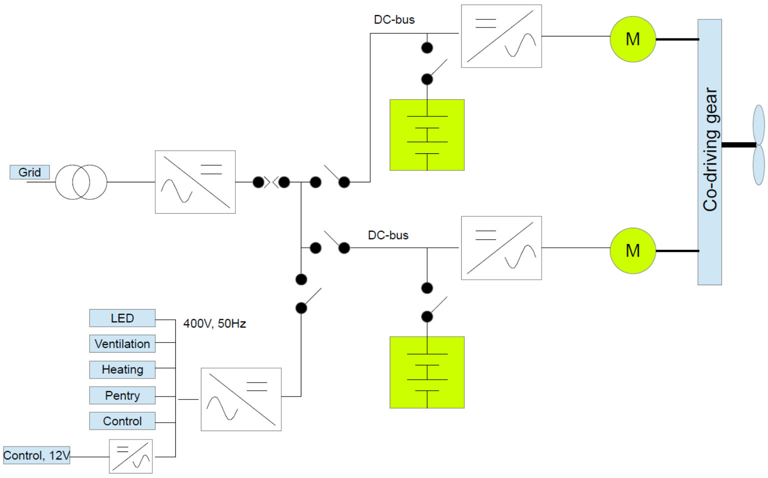

Figure 2. Line diagram of the considered theoretical battery electric passenger ferry.

There are several types of marine **charging solutions** on the market utilizing manual, remote-controlled or automatic connection. The time required to initiate the charge stated by providers of automatic connection range between 10s to 60s (Stemmann-Technik, 2024, Cavotech, 2024), whereas it is 2-4 minutes for remote-controlled connection (Cavotech, 2024). For high power DC chargers, power levels range between 0.5-6.6 MW and voltage levels are commonly 1000 V, 1100 V or 1500 V (Stäubli, 2024), (Cavotech, 2024), (Zinus, 2024), (Stemmann-Technik, 2024). The charging power and strategy was determined in connection with battery sizing.

Operational data

Vesta is one of six ferries to operate in Gothenburg's southern archipelago, taking turns to cover four public transport lines under Västtrafik, where Vesta operates on three of them, and its pattern of movement is rather complex, as shown in ***Figure 3***.

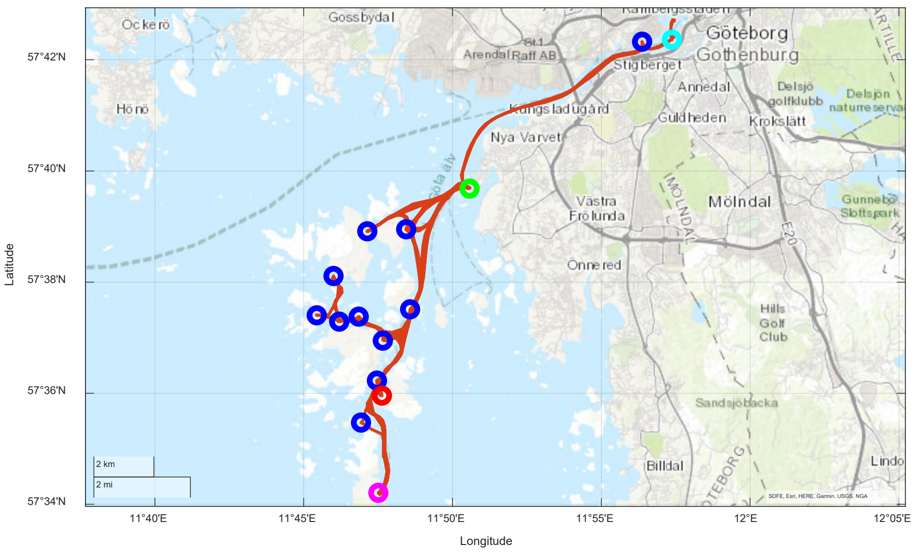

Figure 3. An example of Vesta operation over the course of 90 hours during the winter of 2023. The circles mark visited stations, where green is Saltholmen (Land 1), cyan is Stenpiren (Land 2), magenta is Vrångö (Island 1) red is Donsö (Island 2), and the blue ones are the rest of the visited stops.

There is one timetable valid from the beginning of June to the end of August and one for the rest of the year. In each of the seasonal timetables, Vesta's route of operation is different for Mondays to Thursdays, Fridays, Saturdays and Sundays, even though Vesta's timetable for Mondays-Fridays is shared until around 7 pm. The ferry is visiting land stops three to six times a day. During Mon-Fri in the winter timetable, there are three longer stays in Saltholmen (2 x 0.5 h, 1x 2.5h), and one longer stay at Stenpiren (50 min). In the summer timetable, Vesta has five longer stays in Saltholmen (1x14 min, 3x20 min, 1x 1.5 h) and one at Stenpiren (2h 45 min). Vesta's night rest is at Donsö and the duration varies between 6 h and 13 h, depending on weekday and seasonal timetable.

Operational data, logged with 1 Hz time resolution, was acquired for three days in late October 2021 (Friday, Saturday and Sunday), 2.5 days in late January 2022 (1/2 Friday, Saturday and Sunday) and two days in June 2022 (Midsummer eve operating as Saturday, Midsummer day operating as Sunday) (Styrsöbolaget, 2022). The data contained time stamp, speed above ground, engine volume fuel consumption, as well as engine rotational speed and percentage load. The position data was not included, hence the time stamp and speed data were compared to timetables to determine the location of the visited stops. Due to the storm Malik, which passed during the January's Saturday and Sunday, Vesta covered for other more wind-sensitive ferries, deviating largely from its timetable. There were also a few timetable swaps noted between ferries during the June logs.

To limit the complexity in the project, all time-dependent evaluations are done based on the log of October's Friday, which is thus assumed to be a typical operation. Since the speed above ground was to be the input to ship resistance estimates in calm water, the speed was limited to the maximum speed of the ferry, as shown in *Figure 4*. Furthermore, the first and the last operations of the day represent transportation from and to night rest at Donsö, whereas the timetable start of the day is at Brännö Rödsten, and end of the day is at Styrsö Bratten.

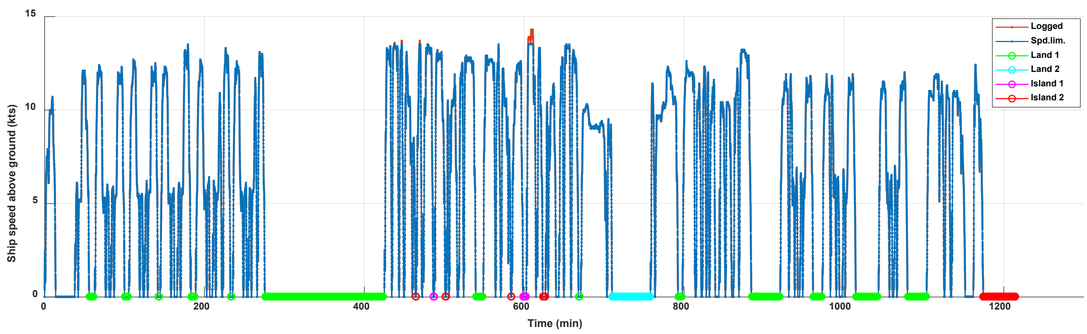

Figure 4. Ship speed above ground, based on log from a Friday in end of October 2021, along with indication of selected stops (notation as in Figure 3).

Estimation of ship resistance

To operate at a certain ship speed, the mechanical output power from the propulsion engine, P_B, must cover for the ship's resistance as well as the combined efficiency of the gear box and shaft, the propeller and its interaction with the ship's hull. The relations are typically written as

$$P_B = \frac{R_T V}{\eta_S \eta_H \eta_O \eta_R}$$

Energimyndigheten

where R_T is the ship resistance (N), V the ship speed (m/s), η_S the shaft and gearbox efficiency, η_H the hull efficiency, η_o, the open water propeller efficiency, and η_R the relative rotative efficiency.

Starting with the ship resistance, it depends on the shape and surface roughness of the hull, displaced water and ship speed, but naturally also conditional factors such as winds, waves and currents. The calm water ship resistance was here estimated using the empirical method Holtrop-Mennen[3](Holtrop and Mennen, 1982, Holtrop, 1984), and for comparative purpose also the rather rough Admiralty law (Aldridge, 2019). To account for weather effects, a sea margin of 15% was used during the drive system's dimensioning.

The Holtrop-Mennen (HM) method require several hull specific parameters as input to empirical equations which are based on statistical and regression analysis from several series of measurements on various model and full-size ships. The method accounts for flat-plate frictional resistance, R_F, a hull form factor, $(1+k_1)$, wave-making and braking resistance, R_W, if applicable an added resistance due to an appendage, R_{APP}, bulb, R_B, and immersed transom, R_{TR}, as well as a model-ship correction factor, R_A. Vesta has no bulb, and the immersed transom was assumed small and thus neglected, thus R_B and R_{TR} were set to zero, which gives the total ship resistance

$$R_{F,HM} = R_F(1 + k_1) + R_{APP} + R_W + R_A$$

Three of the resistance's part contributions; R_F, R_{APP}, R_A (N) follow the general relationship

$$R = \frac{1}{2}\rho C A V^2$$

where ρ is water density (kg/m^3), C is a hull shape dependent coefficient (-), A is a wetted surface area (m), V is the ship speed (m/s). Hence, their contribution to the total resistance increases with the square of the speed.

Furthermore, the studied ferry's hull specific parameters such as draught, T, block coefficient, C_B, waterplane area coefficient, C_{WP}, prismatic coefficient, C_P, longitudinal position of the centre of buoyancy, LCB, and projected wetted surface area, A_{WS}, were all modelled as function of displacement based on data in the ship's stability book. The resulting components of ship resistance for the studied ferry is presented in *Figure 5*. Below around 12 knots $R_F(1+k_1)$ dominates, whereas at higher speed levels R_W dominates.

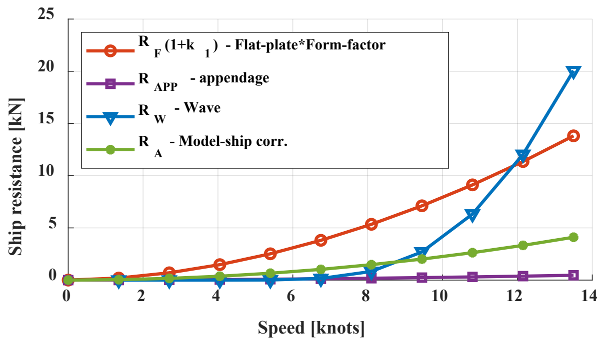

Figure 5. Components of estimated ship resistance using HM for the studied ferry-concept, as a function of ship speed.

[3] Alternative empirical methods such as Hollenbach or Guldhammar and Harvald were not suitable as the studied ship parameters exceeded their range of applicability, which are typically much larger vessels for good transportation.

To evaluate the accuracy of the HM result, a model test could be conducted, however such an effort was considered out of the scope in this project. A second-best alternative could be a comparison with computational fluid dynamics (CFD). However, since the detailed hull shape is not known and the expected time consumption for such modelling and simulation would still be rather high, it was also considered out of the scope.

The rougher Admiralty law can be used to relate the maximum engine output power, P_B (kW), at full mass displacement, Δ (ton), and top ship speed, v (knots), via the hull shape dependent Admiralty coefficient, A_{adm}, as

$$P_B = \frac{\Delta^{2/3}\, v_{ship}^3}{A_{adm}}$$

Thus, with P_B as in the diesel-powered version of Vesta and displacement at full load (see *Table **1***), the A_{adm} can be found and used to estimate the full load ship resistance as a function of speed. However, in practice A_{adm} may only be approximated as constant for small variations in speed, or the ship resistance may be overestimated (Kim et al., 2023).

The calm water total ship resistance from using the HM method with light and with full weight with/without sea margin, as well as the resistance from using the Admiralty law are shown in *Figure **6***. Provided that the current propulsion system is likely dimensioned with a certain sea margin in mind, the resulting resistance at top speed from using HM and a 15% sea margin was considered acceptably representative for this study.

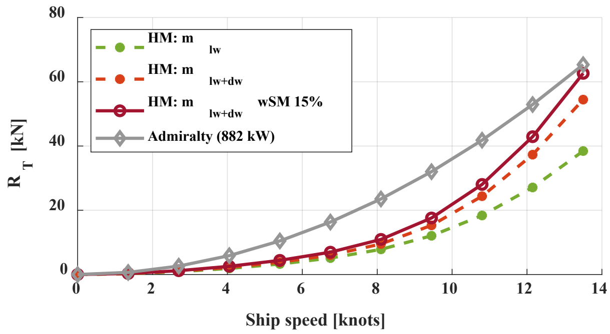

Figure 6. Estimated ship resistance as a function of ship speed using HM with the concept ferry's light (m_{lw}) respectively full weight (m_{lw+dw}) and with full weight and a 15% sea margin, as well as the resistance using the Admiralty law based on Vesta's installed engine output power.

Estimation of hull and propeller efficiency

The hull efficiency or coefficient, η_H, describes to what extent the shape of the hull increases or decreases the required propulsive power of the ship. It is thus not a formal efficiency, since it for many ships exceeds one, i.e. reduces the needed propulsive power. Here, the hull efficiency is estimated via the so-called wake fraction and thrust deduction coefficients, w, and t. These parameters were estimated as suggested by the HM method (Holtrop, 1984), where w has a speed dependency, giving an average hull efficiency around 97.9%, thus the hull shape increases the required propulsion power somewhat.

Also, the relative rotative efficiency, η_R or coefficient, was approximated using the HM suggested method to 99.7%, which can be deemed realistic as it is usually around 1 or slightly above for single propeller ships (MAN, 2023).

The open water propeller efficiency, η_O, assumes there is no hull in front of it, and it depends on propeller-related factors such as its diameter, number of blades, expanded area ratio, pitch-to-diameter ratio, rotational speed and thrust force (MAN, 2023). The only known parameters are the blades number and maximum rotational speed, *Table 2*. The diameter, D_{prop}, was estimated based on ship drawings to be 1.75 m. The expanded area ratio was estimated using the HM suggested method (Holtrop, 1984) to be around 0.71, which is in the higher range. The open water propeller efficiency also depends on the speed of the water to the propeller, which is often express via the dimensionless parameter speed of advance, J, here approximated to around 0.52 at top speed.

As there is no analytical method, the open water propeller efficiency was approximated with help of the Wageningen B-screw series, which is commonly used (Carlton, 2007). Required input parameters are propeller diameter, number of blades, expanded area ratio, as well as the pitch-to-diameter ratio. For the latter, 0.93 was identified as a beneficial choice in terms of efficiency, using an industrially developed interpolation tool which combined the B-series data with empirical data on several propeller designs (BERG Propulsion, 2022-2024). With the same tool, an approximate open water propeller efficiency was then determined to 51.6%. For electric propulsion, a fixed blade pitch was considered reasonable, in which the propeller power is regulated only with its speed. By doing so, η_o could be considered as constant. For simplicity, the fuel consumption of the diesel-powered ship was also modelled with the same fixed pitch, and efficiency.

With an approximate shaft and gearbox efficiency of 97%, the total propulsive efficiency at full load and top speed was

$$\eta_{prop} = \eta_H . \eta_o \cdot \eta_R \cdot \eta_S = 97.9\% \cdot 51.6\% \cdot 99.7\% \cdot 97\% = 48.8\%$$

In Part 3 of the project, operational fuel and energy consumption was targeted, using drive system component models of fuel and energy consumption as a function of torque and speed. Thus, from the input ship speed, a shaft speed was sought, i.e. the propeller speed. For this, an industrially developed graphical representation was utilized showing the ship's approximated propeller load curves as functions of propeller speed, including indications of ship speed. As mentioned, a fixed blade pitch was assumed. Then a relation between ship and propeller speed was deduced as the red line in *Figure 7*, which also shows logged data as a comparison. In the actual ship, the propeller speed was kept rather constant up to around 10 knots, above which it varied with ship speed and perhaps propeller blade pitch.

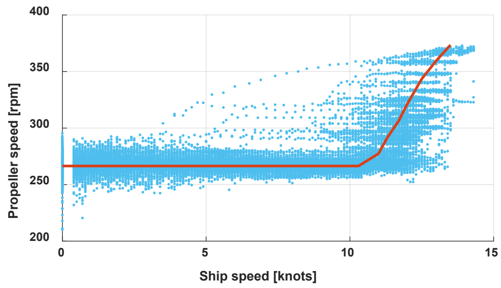

Figure 7. Derived propeller speed as a function of ship speed, (red) as used in propulsion simulations in Part 3 of the project, (blue) logged data the October's Friday.

Determining operational profile

Using the determined calm water ship resistance and propulsive efficiency, the needed motor output power was established with a fully loaded ship and an additional 15% sea margin to account for rough weather, as shown in *Figure 8*. The resulting required propulsion power was around 895 kW, which is close to the currently installed total engine power of 882 kW.

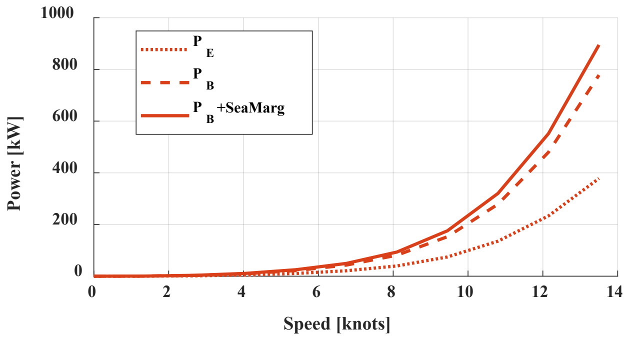

Figure 8. Estimated required engine propulsion power, P_B, at full load, w/wo sea margin of 15%, along with required towing power, P_E, both as functions of ship speed.

In the same way, the time series of calm water propulsion power was established and compared to the logged engine power, which revealed missing components of representation at both low and high ship speed. For better coherence at high speed, a positive acceleration force was included, simply by using Newton's 2nd law of motion. Low-speed operation occur when the ferry is approaching a stop. Then it decelerates, activates the bow thruster for improved manoeuvring capability, and when reaching the dock starts pushing against it, still using the bow thruster to keep the ship straight. When leaving the dock, it reverses the speed and turns, then halts, deactivates the bow thruster and accelerates to service speed. Based on the propulsion power of the October's Friday log, low-speed operation was divided into four modes, for which the average used propulsion power was determined, as stated in *Table **3*** and illustrated in *Figure **9***. Therefore, during low-speed operation, the determined calm water required propulsion power was replaced with the defined power levels for respective mode of operation.

Table 3. Imposed propulsion power for low speed amd manoeuvring operation.

Speed range	Operation mode	Propulsion power
5-8 knots	Low speed manoeuvring	120 kW
<5 knots	Reducing speed	223 kW
0 knots	Pushing to dock	175 kW
<5 knots	Low speed acceleration	313 kW

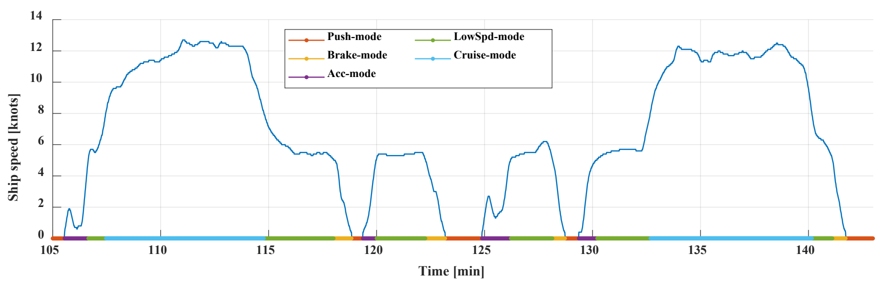

Figure 9. Example of defined modes of operation.

The resulting estimated propulsion power with full load in calm water is shown in *Figure **10***, along with logged engine operation and maximum power curve, as a comparison. Note the passenger loading and weather conditions of the logged data is unknown.

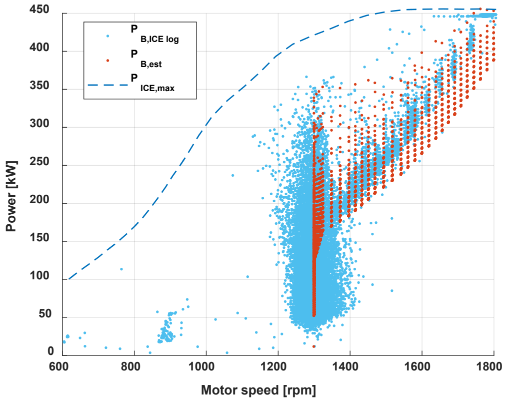

Figure 10. For October's Friday speed profile, (red dots) Estimated calm water propulsion power as a function of motor speed, (blue dots) logged enigne operation, and (blue dashed line) engine maximum power.

Dimensioning of electric motor

The total electric motors' rated power was chosen to be 900 kW (i.e. 2x 450 kW), as rounded from the predicted top speed power requirement with sea margin. Furthermore, the motors' top speed was targeted to 1800 rpm, i.e. the same as the engines' top speed.

If the motor's rated speed would be 1800 rpm, it would imply a rated torque of around 2400 Nm per motor. However, the peak torque of the diesel engines is around 3000 Nm, and logged engine operations revealed the actual use of such torque levels, as shown in *Figure **11***, likely representing pushing against the dock. For simplicity, thus the electric motor's continuous/rated torque was set to 3000 Nm, which with the power of 900 kW, gives a base speed of around 1432 rpm. The electric motor's targeted continuous torque envelop is also shown in *Figure **11***. The motor power was targeted for an anticipated minimum dc-bus voltage.

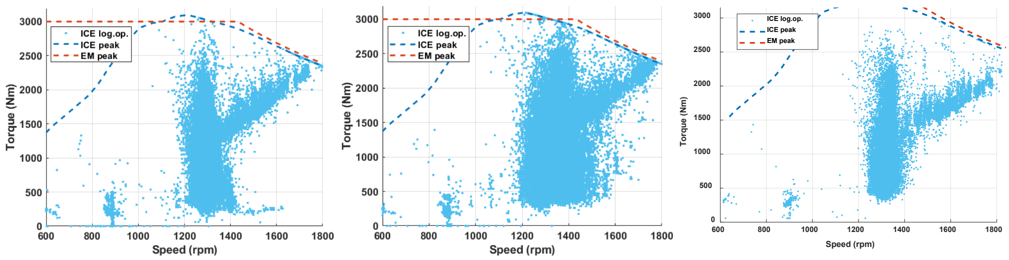

Figure 11. Derived diesel engine (ICE) operating points of logged days in October 2021, January 2022 (with two stormy days) and June 2022 along with engine peak torque and chosen electric motor peak torque.

The resulting estimated electric motor operating points are shown in ***Figure 12***.

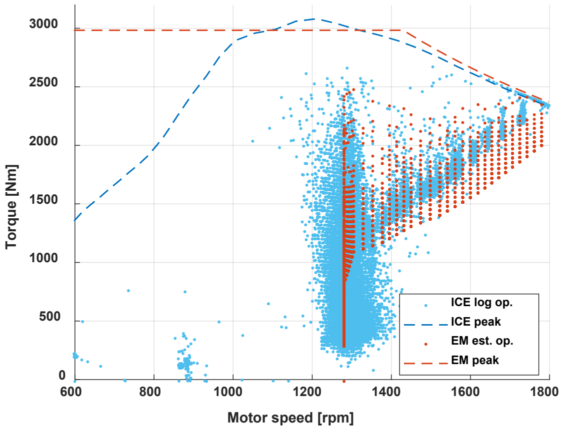

Figure 12. Estimated electric motor operating points for the October's Friday ship speed above ground, with full load in calm water, along with the peak electric motor torque, as well as derived engine operation from logged data and peak engine torque.

Early dimensioning of battery and charging

To get an insight into the demands on the battery capacity and a suitable charging strategy, an early battery dimensioning process was conducted. Then, the battery energy requirement was determined using the operational data shown in *Figure **4***, i.e. the October Friday's route, the estimated ship resistance (without sea margin, it was added later), propulsive efficiency, and constant drive system components efficiencies; 95% for electric motors, 97% for inverter and battery. In addition to propulsion, 75 kW electricity for heat pump (space heating) and 60 kW for auxiliary loads were considered drawn from the battery.

To start with, the mass of the fully loaded diesel propelled version was used. Then, if the battery ran all day without charging, the consumed battery energy would reach 4.9 MWh (usable capacity), which implies an even larger installed battery capacity (around 8.0 MWh installed).

To reduce the required battery size, high power opportunity **charging** at the most visited land-stop Saltholmen (Land 1) was considered, as well as at the land-stop Stenpiren (Land 2) which had a scheduled stay of around 50 min. Both stations were considered equipped with identical 4 MW charging solutions at this stage.

Since Vesta's night rest was at Donsö (Island 2), there is a natural reason for a charger there. Due to anticipated limited power transfer in sea cables, a lower charge power was considered compared to the land stations; i.e. 0.5 MW.

For dimensional purpose, a simplistic battery modelling was used with specified energy capacity, energy consumption as the time integral of battery power, and estimated relative level of energy as indication of state of charge (SoC). The starting SoC as well as upper limit during charging, was set to 85%.

The most demanding segment, which thus set the dimensioning requirement for the battery, was the operation between time stamp 425 min, to 711 min, i.e. from mainland Saltholmen (Land 1) down to Vrångö (Island 1) and back, twice in a row, followed by a trip to Stenpiren, indicated by the orange rectangle in *Figure **13***. In the exemplified scenario in *Figure **13***, the consumed battery energy within the rectangle, was 1.7 MWh. To acquire a full battery energy rating, a SoC window between 85% down to 15% was assumed, and a margin for rough weather of 15% was added. Then, for a usable energy of 1.7 MWh, an installed battery capacity of 2.8 MWh would be required.

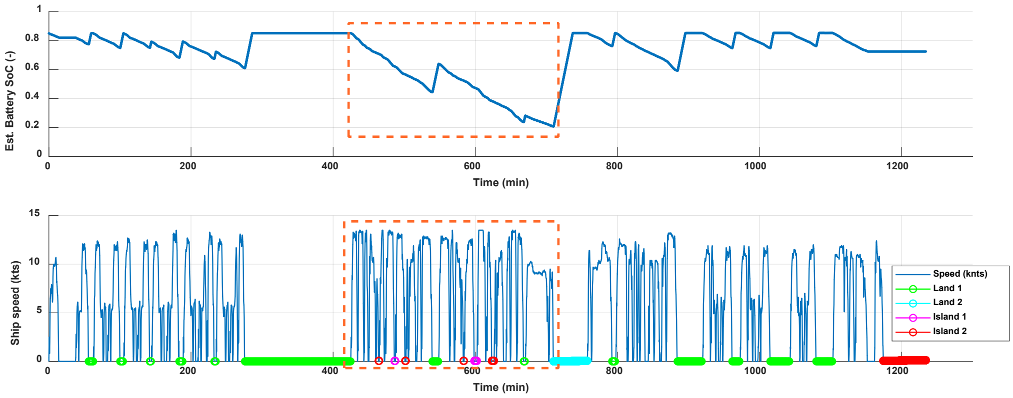

Figure 13. Simplistic SoC estimation, ship sped, and indication of stops identified as potential charging stops. Orange rectangel mark sequence of operationa which was dimensioning of the battery pack. Here, exemplified with full load, with 2.8 MWh battery and 4 MW charging at Land 1 and 2.

Since the energy required for propulsion is influenced by the weight of the ship, the ship mass was modified for the retrofitted version. The weight of the main engines, motor oil, exhaust after-treatment system and exhaust pipes, the auxiliary genset, and the oil heater were estimated to around 8.1 tonnes, and the bunkers to around 14.9 tonnes. The former reduced the light weight and the latter the dead weight, in total a reduction of 23 tonnes. For the battery electric ship version, the weight of electric machines, power electronic converters, cables, fuses, brakers and a heat pump were estimated to add around 4.5 tonnes. For simplicity, the engine cooling glycol system was assumed to remain for the electric drive and battery system, or anyway not contribute to a relevant change of weight.

However, the main weight addition to the retrofitted ferry was due to the battery, which adds to the ship's light weight. In the early battery dimensioning process, there were two aspects to consider. Firstly, the energy density of LFP and NMC battery types differ, thus so will the corresponding ship mass and resulting energy consumption. Secondly, the required battery energy capacity and the battery mass are codependent. Therefore, the battery energy content and weight were determined in an iterative process. With a starting battery energy content and mass, the critical ship energy consumption was determined, whereupon the required battery energy capacity and mass were updated for a second run. The process was repeated until the change in required battery energy capacity was less than 1%. The reached battery dimensions are given in *Table* 4.

Table 4*: Early estimation of usable and installed battery energy capacity of October's Friday route, and battery pack mass.*

Battery type	Required usable energy (MWh)	Required installed battery capacity (MWh)	Battery pack mass (ton)
NMC	1.681	2.762	17.5
LFP	1.708	2.806	22.0

Energimyndigheten

Part 2 - Electric motor, inverter and battery modelling

Load dependent power loss and efficiency models were established for the electric motors, inverter and battery.

Electric motor electromagnetic modelling

Two electric motors were modelled: one PMSM and one SRM, sharing the same stator construction, but having different rotor constructions. For the PMSM, the geometry cross-section, materials, electromagnetic modelling and two-dimensional (2D) finite element analysis (FEA) were the same as for the automotive Nd(Dy)FeB[4] PMSM treated in previous LCA publications (Nordelöf et al., 2017, Nordelöf and Tillman, 2017). It means sinusoidal current excitation, and a copper and magnet temperature of 70ºC. However, the radial dimensions and stack core length were enlarged for the higher power rating, as were the voltage and current ratings. The SRM has the same stator geometry and materials as the PMSM, which enables the use of the same life cycle inventory while excluding magnet related parts.

The stator outer diameter was set to 480 mm, with 48 slots, 8 poles, a two-layer winding in four parallel branches, with a 0.45 copper fill factor. Diverging machine specifications are listed in *Table **5***. Since the dc-bus voltage was set to vary with battery loading, so will the electric machine output power, such that a higher dc-voltage with allow a higher output power. The machines' current rating, or coil current density, depend on the chosen cooling solution. Relatively low current densities were used in both machines, to avoid risk of overheating. Thermal modelling and simulations were considered out of the scope in this project. The implemented models are shown in *Figure **14***.

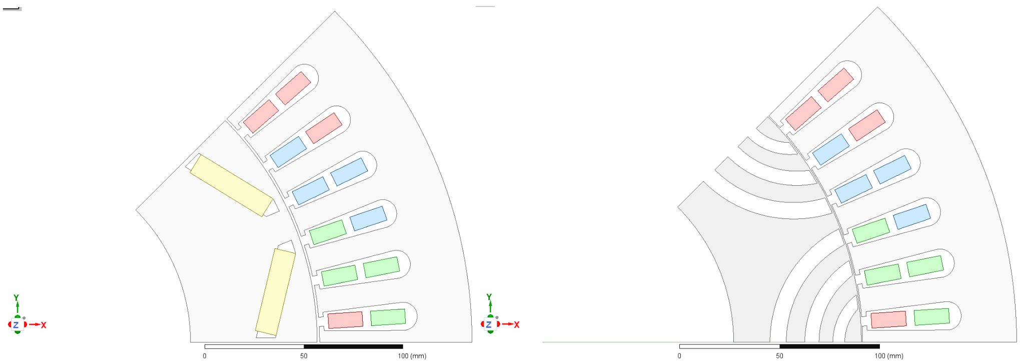

Figure 14. One pole (45º of the full 360º) cross section of the (left) PMSM, (right) SRM. Stator phase windings are blue, green and red, magnets in PMSM are yellow, air pockets are white.

The FEA determined core losses were here post-compensated by a factor of 1.7, since there is typically a gap between FEA and experimental determined core losses. Often stated reasons are the two factors of steel sheet stamping during manufacturing and switched power electronic converter feeding, which are both prone to increase the core losses, however, not considered in the FEA. Furthermore, the winding losses are compensated for estimated contribution due to the end-windings.

The torque production capability in the SRM was as expected lower than in the PMSM, hence its core stack is prolonged by 57% to compensate, thus its total mass is 26% higher. The resulting efficiency as function of torque and speed are shown to the left and in the middle in *Figure **15***, along with the LCA use-phase operating points.

[4] Neodymium dysprosium iron boron (Nd(Dy)FeB

Table 5. Selected electric machine specifications.

	PMSM	SRM
Stator outer diameter	480 mm	480 mm
Stack length	217 mm	340 mm
Turns per coil	8	6
Rated rms current	720 A	745 A
Rated rms current density	11 A/mm^2	8.5 A/mm^2
Peak efficiency	97%	95%
Rated torque	3001 Nm	3001 Nm
Rated power	450 kW	453 kW
Base speed, @ V_{dc}	1432 rpm, 750 V	1443 rpm, 700 V
Estimated total weight	455 kg	575 kg

Inverter power loss modelling

The heart of the motor inverter is its power module, which contains switches realized by transistors and diodes. In this work, a two level IGBT power module was used, FF900R17ME7W_B11(Infineon, 2024), which enables the life cycle inventory from (Nordelöf et al., 2018) to be utilized in the inverter wheel-to-tank part of the LCA. For the LCA use-phase, the power losses in the power module are modelled as in (Arfa Grunditz and Thiringer, 2018), including IGBT on-state, turn-on and turn-off losses as well as the diodes on-state and turn-off losses. A switching frequency of 3 kHz was used. The power module's peak efficiency was then 99%.

The chosen rating of the power module was 1700 V and 900 A, to allow for temporary over voltages and short time currents. To make sure a chip temperature of 150°C would not be exceeded, the transistor and diode temperatures were estimated at data sheet cooling conditions (60°C coolant, 10L/min). In the operating area for the ferry, the diode temperature did not exceed 100°C, and the transistor reached around 130°C at most. The resulting efficiency is shown to the right in Figure 15, along with the LCA use-phase operating points.

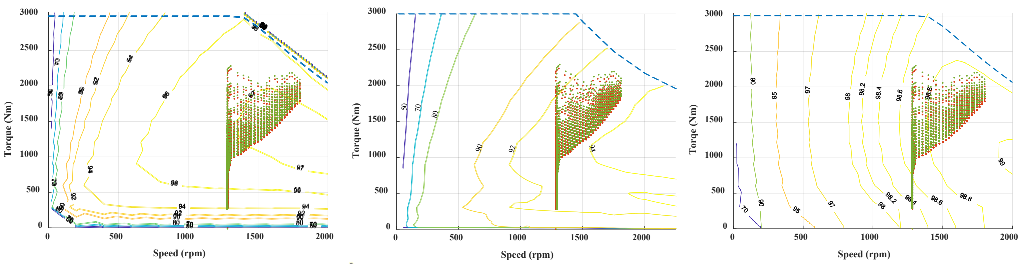

Figure 15. Efficiency of one (left) PMSM electric motor, (middle) SRM electric motor, (right) motor inverter as a function for motor torque and speed, along with operating points for the LCA use-phase batteries (red) NMC-1 Mid and (green) LFP-Mid-1 case, from Part 3.

Battery modelling

Two different battery models were used in the project: one to calculate battery design and material consumption, and one to calculate battery performance. The models were constructed in a previous project and have been further developed in this project (Chordia et al., 2022). The *battery-design model* was built in Matlab and has been used to calculate the basis for the life cycle analysis regarding the choice of material, material consumption, weight and volume. It also provided design parameters that were used in the battery-performance model. The *battery-performance model* was built in COMSOL, and the results were used to design battery packs and calculate battery power losses during the LCA use phase.

Two different **battery chemistries** were investigated. Both variants used graphite as the negative electrode. The two different positive electrode materials were the nickel-rich material NMC622, with high energy density, and the LFP, with a lower energy density. A larger prismatic cell format, BEV2, was selected and the design-model was used to calculate possible cell designs. Each battery chemistry has been investigated using three different design targets: energy-optimized, power-optimized and an intermediate design. The designs' different material consumption and type served as input to the life cycle evaluation in Part 4 of the project. The COMSOL performance model uses the built-in material library for NMC622, LFP and graphite to estimate the performance. The performance was used in project Part 3, when establishing the energy consumption of the battery electric ferry.

Battery cell design and performance

The three different cell designs for the two different battery chemistries in the prismatic format BEV2. A BEV2 cell is 12.6 cm high, 17.4 cm wide and 4.5 cm thick and has a volume of 0.987 l. Typically, larger prismatic cells contain several smaller battery rolls, so-called jellyrolls, that are all connected to the terminals of the cover. In this design, 4 jellyrolls were adopted and based on the available volume and the thickness of an electrochemical cell, where the length of the jellyroll was calculated using Archimedes spiral. A manuscript describing the design model is in preparation.

The mass breakdown for the different components in the six different cell designs are included in *Figure **16***. The power optimised designs results in a heavier cell compared to the energy optimised designs. The detailed cell mass breakdown is included in *Table **16*** and *Table **17*** in Appendix B. The fraction active materials are lower in the power optimised and the fractions for separator and current collectors higher. This is a result of the power optimised design, where the electrode layers are very thin, with low surface capacity, but compensated by a large surface area.

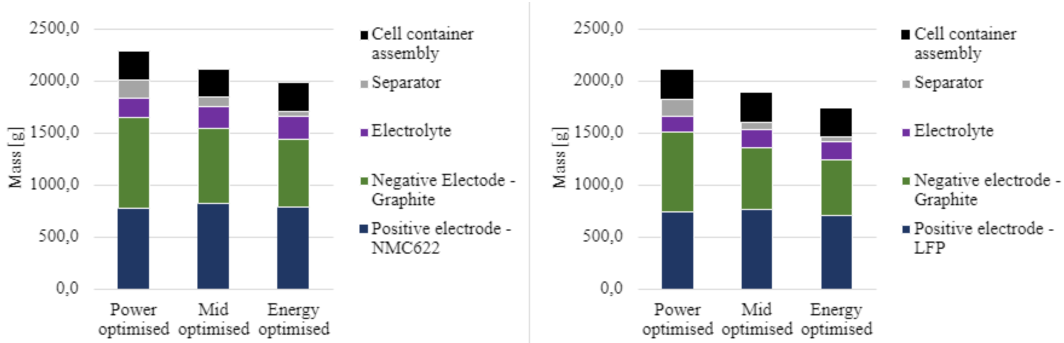

Figure 16: Cell component mass breakdown of the designs for the NMC622-Graphite cells to the left and the LFP-Graphite cells to the right.

In the battery design model, the cell capacity is estimated and calculated as the product of surface capacity and surface area. The higher the surface capacity of an electrode, the higher the possibly achievable gravimetric energy density. As can be seen in *Table **18*** and *Table **19***, the medium-optimized cell has higher capacity than the energy-optimized cell, for both chemistries. This is due to achieving a higher fill factor of the prismatic casing, which can be seen in the volumetric energy density. An example to visualize this is included in *Figure 17*.

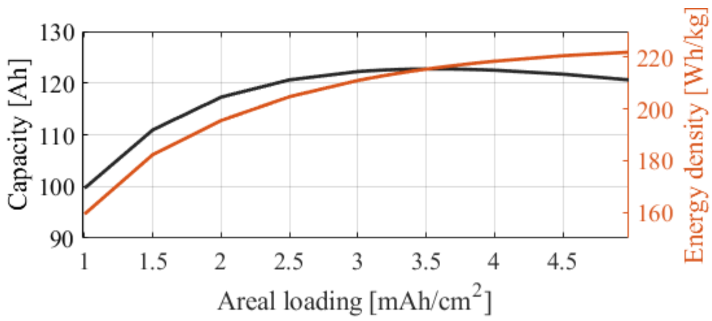

Figure 17. Cell charge capacity and energy density as a function of areal loading.

In the performance model, the cell capacity is simulated with a 0.1C discharge rate between the maximum and minimum voltage. The output design from the cell design model is used as input to the COMSOL performance model together with some additional design parameters needed for the COMSOL model. Input data from the design model and simulation results are included in *Table **18*** and *Table **19*** in Appendix B.

The performance simulation includes a rate test for charge capacity and C-rate capability, and a pulse test for resistance estimation. An example of the simulated results from the C-rate test of the two Mid designs are included in *Figure **18**Figure **18**: Simulation results from the rate test on the Mid optimised designs. Solid line is NMC-Graphite and LFP-Graphite is the dashed lines.*. It can be seen that the charge capacity is dramatically reduced when discharging with C-rates above 5C, indicating the maximum rate capability. The simulation results were used for the battery pack design and loss calculation during usage.

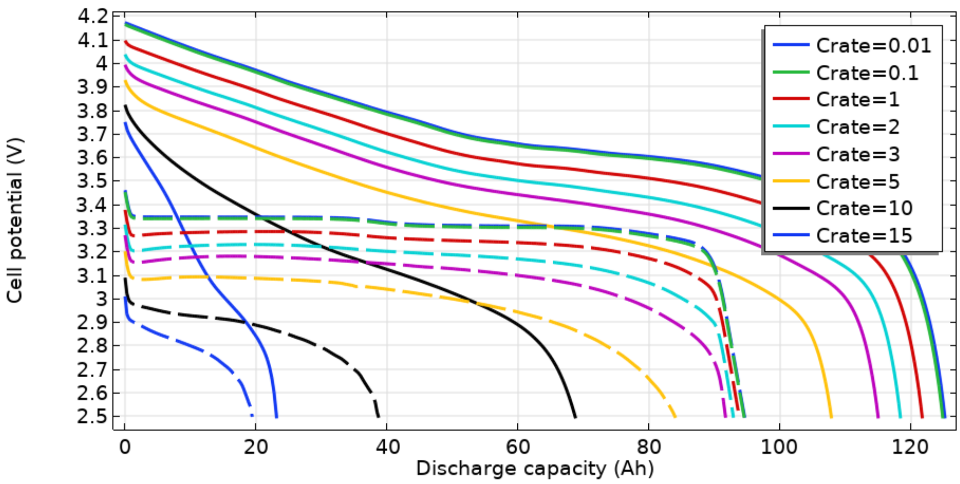

Figure 18: Simulation results from the rate test on the Mid optimised designs. Solid line is NMC-Graphite and LFP-Graphite is the dashed lines.

Final battery pack design, performance and charging

The early battery dimensioning served as input in the final battery dimensioning when considering the integer number of cells in series connected strings and number of parallel connected strings. The number of series connected cells were determined by a voltage

Energimyndigheten

requirement of reaching 950 V at 85% SoC. Then the number of parallel strings were determined both due to the required energy and charging power, while making sure the SoC during did not reach lower that around 15%-18% during operation with a fully loaded battery electric ferry and a 15% sea margin. By varying the used charging power and the desired installed energy, the combination which gave the lowest number of parallel strings was chosen. To make sure the resulting pack configuration could handle even more severe weather conditions, a sea margin of 35% was also tested while relaxing the minimum SoC to 1%. A maximum charging power of 4 MW was used.

As for the early dimensioning process, this too was iterative, as a given pack design correspond to a certain battery weight, which in turn affects the ferry's light weight. The pack weight was determined based on the cell-level weight and a multiplication factor of around 1.33 for NMC and 1.37 for LFP batteries, as determined in Part 4 of the project.

The six different battery types have different strengths and weaknesses, which leads to different optimal designs. The energy-optimized cells are limited by the fact that they cannot handle fast charging. The power-optimized and mid-optimized cells have no problem coping with fast charging, instead it is the charging infrastructure that limits the charging. The procedure was repeated for the three different cells of the two chemistries. The resulting battery pack's design and performance when using today's timetable as design requirement, called Charging Scenario 1 (CS1), are presented in *Table 6*.

Generally, the NMC-packs have lower mass compared to the LFP-packs, and somewhat lower required installed energy. The energy optimized cells required the highest installed energy, whereas the power optimized cells lead to the heaviest battery packs. For both chemistries, the Mid-optimized packs offered the lowest installed energy and pack weight, which is why they were chosen to be included in the LCA.

Table 6. Battery pack design with today's timetable, CS1, with dimensioning-case operation data.

	Pack performance	Unit	LFP Power	LFP Mid	LFP Energy	NMC Power	NMC Mid	NMC Energy
Design	Energy install.	MWh	2.72	2.65	3.03	2.67	2.61	3.00
	Capacity install.	kAh	2.9	2.8	3.3	3.1	3.0	3.4
	Series cells		284	284	284	239	238	238
	Parallel strings		18	15	18	15	12	14
	Weight	ton	29.4	22.0	24.3	21.8	16.1	17.6
	Volume	m^3	14.4	12.0	14.4	10.1	8.1	9.4
	Specific energy	Wh/kg	92.6	120.5	124.8	122.8	162.6	170.9
	Energy density	Wh/l	188.8	220.2	210.5	264.5	324.2	319.5
	Max. voltage	V		1037		1004	1000	
	Min. voltage	V		710		598	595	
	Pack resistance	mΩ	5.1	6.8	7.4	8.5	9.6	9.4
	Peak power	MW	13.6	7.9	3.1	12.4	7.3	2.9
	$C\text{-rate}_{max}$		5C	3C	1C	5C	3C	1C
Dim. Op.	$\text{Charg. Power}_{Land}$	MW	4.0	4.0	2.4	4.0	4.0	2.7
	$\text{Charg. C-rate}_{max}$		1.44	1.47	0.78	1.52	1.54	0.91
	$\text{Disch. C-rate}_{max}$		0.45	0.45	0.39	0.44	0.44	0.39
	Reached SoC_{min}	%	16%	16%	16%	16%	15%	17%

To further reduce the battery sizes, a change in operation was investigated. As mentioned in Part 1, the most critical part of the operation when it comes to battery dimensioning, was the round trip from mainland Land 1 (Saltholmen) to Island 1 (Vrångö) and then further on to Land 2 (Stenpiren). Therefore, the effect on needed installed battery energy was investigated when allowing a longer stop after the first of the two roundtrips. Thus, a second charging scenario, (**CS2**) where the charging time at Land 1 was doubled from around 9.5 minutes in CS1, to 20 minutes in CS2.

The resulting Mid-battery pack designs are presented in *Table 7*. For both chemistries, a battery weight reduction of 33% was reached. For the LCA use-phase operation, the number of cycles the batteries will conduct per day is presented in full cycle equivalents (FCE). This is a measure of the current throughput (both charging and discharging) over two times the nominal installed capacity.

Table 7. Battery pack design with CS1, CS2, with operation data during the LCA use-phase.

	Pack performance	Units	LFP-1 Mid	LFP-2 Mid.	NMC-1 Mid	NMC-2 Mid
Design	Energy installed	MWh	2.65	1.76	2.61	1.74
	Capacity installed	kAh	2.8	1.9	3.0	2.0
	Series/parallel		284s**15p**	284s**10p**	238s**12p**	238s**8p**
	Weight	ton	22.0	14.6	16.1	10.7
	Volume	m^3	12.0	8.0	8.1	5.4
	Specific energy	Wh/kg	120.5		162.6	
	Energy density	Wh/l	220.2		324.2	
	Max. voltage	V	1036.6		999.6	
	Min. voltage	V	710		595	
	Pack resistance	mΩ	6.8	10.2	8.5	14.4
	Peak power	MW	7.9	5.2	12.4	4.8
	Max. design C-rate		3C	3C	5C	3C
Use ph. op.	Charg. $Power_{Land}$	MW	4.0	4.0	4.0	4.0
	Charg. $C\text{-}rate_{max}$		1.29	1.67	1.27	1.75
	Disch. $C\text{-}rate_{max}$		0.30	0.38	0.27	0.37
	Reached SoC_{min}	%	47.1%	49.1%	49.2%	48.2%
	FCE/day		1.56	1.96	1.45	1.97

The corresponding ship weight is presented in *Table 8*, and shows a general expected full ship weight reduction for the battery electric ferry versions compared to the diesel ferry version. The part-load weight reduction is somewhat less.

Table 8. Corresponding ship weight (ton) for CS1, CS2, with NMC-Mid and LFP-Mid, both full weight and part load weight with 50% passengers, along with the corresponding weight for the ICE ferry version as from Table 1.

	ICE	NMC-1	NMC-2	LFP-1	LFP-2
Fully loaded ship weight	277.1	267.0	261.6	272.9	265.5
	100%	96.3%	94.4%	98.5%	95.8%
Partly loaded ship weight	254.4	250.1	244.7	256.0	248.7
	100%	98.3%	96.2%	100.6%	97.7%

Finally, the time series of the dimensioning-case operation is exemplified in *Figure 19* by the NMC-Mid pack designs for the two charging scenarios.

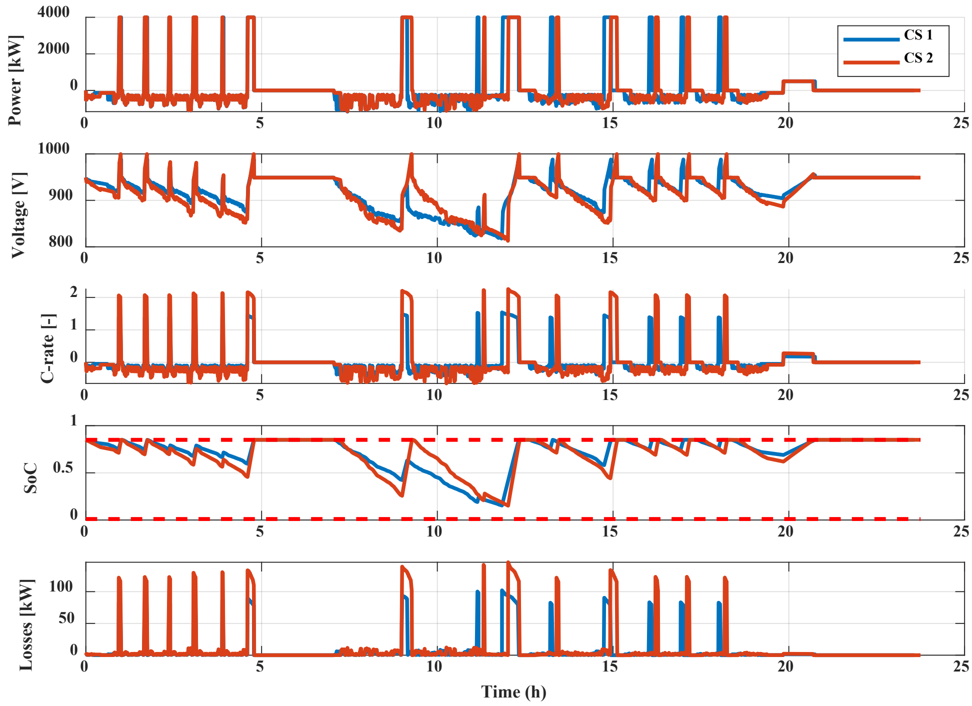

Figure 19. Operation of the two battery packs of NMC-Mid, for CS1, CS2, for the purpose of final battery pack dimensioning, i.e. full ship weight and 15% sea margin.

Part 3 – Quantification of propulsion energy and fuel consumption

The LCA use-phase fuel and energy consumption was determined for a partly loaded ferry, as stated in *Table **1*** for the diesel ferry and in *Table 8* for the battery electric ferry versions. To ensure equal operating conditions in all cases, the propulsion power was determined based on the calm water ship resistance with weight-dependent displacement, whereas the power during low speed and manoeuvring operation was as stated in *Table **3***.

For the electric propulsion case, the auxiliary electric load was still 60 kW, whereas the electric load due to heating was here set to zero. For the diesel propulsion case, both the auxiliary and heat loads were set to zero. These factors were instead included during the life cycle assessment.

Battery electric propulsion

For the case with battery NMC-Mid and LFP-Mid with CS1, the total energy losses in the two different electric machines and the inverter are presented in *Table **9***. The inverter losses correspond to the case of input data of the PMSM. The SRM losses are more than twice that of the PMSM losses. The losses in the inverter are the lowest of the drive system components, followed by the PMSM and then battery losses, whereas the SRM losses are the highest. For the LFP-Mid-1 case, the motor and inverter losses increased around 2% per component, (not shown here), whereas the battery losses reduced by around 29%, compared to the NMC-Mid case.

Table 9. Total energy losses (kWh) and average energy efficiency in electric motors, inverters (for NMC-Mid-1) and in the two different Mid batteries for CS1.

	PMSM	SRM		Inverter		NMC-Mid-1	LFP-Mid-1
$E_{loss,cu}$	38.2	155.4	$E_{loss,cond}$	19.3	$E_{loss,char}$	165.2	116.6
$E_{loss,fe}$	90.9	123.3	$E_{loss,sw}$	29.8	$E_{loss,dischar}$	18.7	13.3
$E_{loss,PM}$	0.3						
$E_{loss,tot}$	129.4	278.7	$E_{loss,tot}$	49.2	$E_{loss,tot}$	184.0	130.0
η_{ave}	96.7%	93.2 %	η_{ave}	98.8%	$\eta_{ave,char/dischar}$	96.6%/ 99.6%	97.6%/ 99.7%

The NMC-Mid battery operating voltage (op.) and open-source voltage (OCV) as functions of SoC are shown in *Figure 20*, and the time series operation of the NMC batteries for the two different charging scenarios are presented in *Figure 21*.

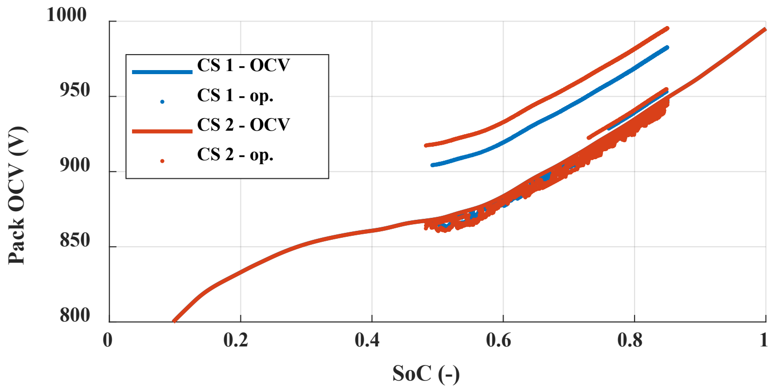

Figure 20. NMC-Mid pack-level OCV and operating voltage as function of SoC, for the two charging scenarios; CS2, CS2 during the LCA use-phase operation.

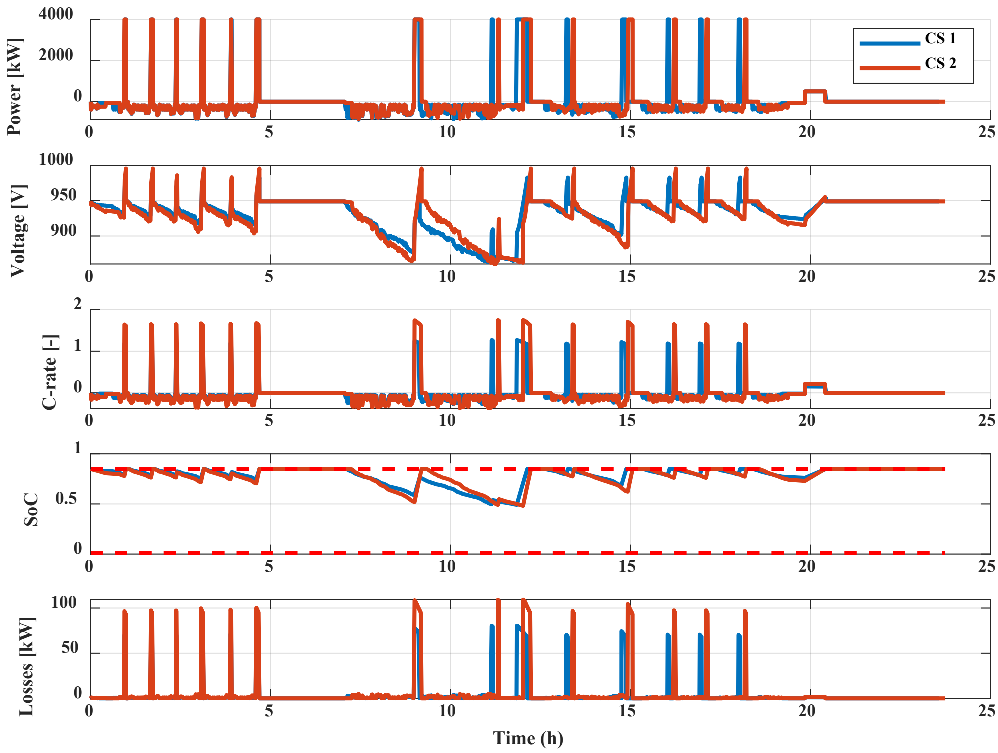

Figure 21. NMC-Mid battery operation with CS1, CS2, during the LCA use-phase operation.

The LFP battery operating voltage (op.) and open-source voltage (OCV) as functions of SoC are shown in *Figure 22*, and the time series operation of the LFP batteries for the two different charging scenarios are presented in *Figure 23*.

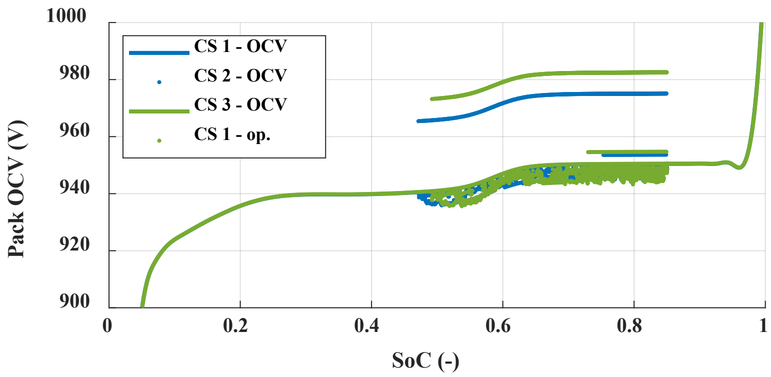

Figure 22. LFP-Mid pack-level OCV and operating voltage as function of SoC, for the two charging scenarios; CS1, CS2, during the LCA use-phase operation.

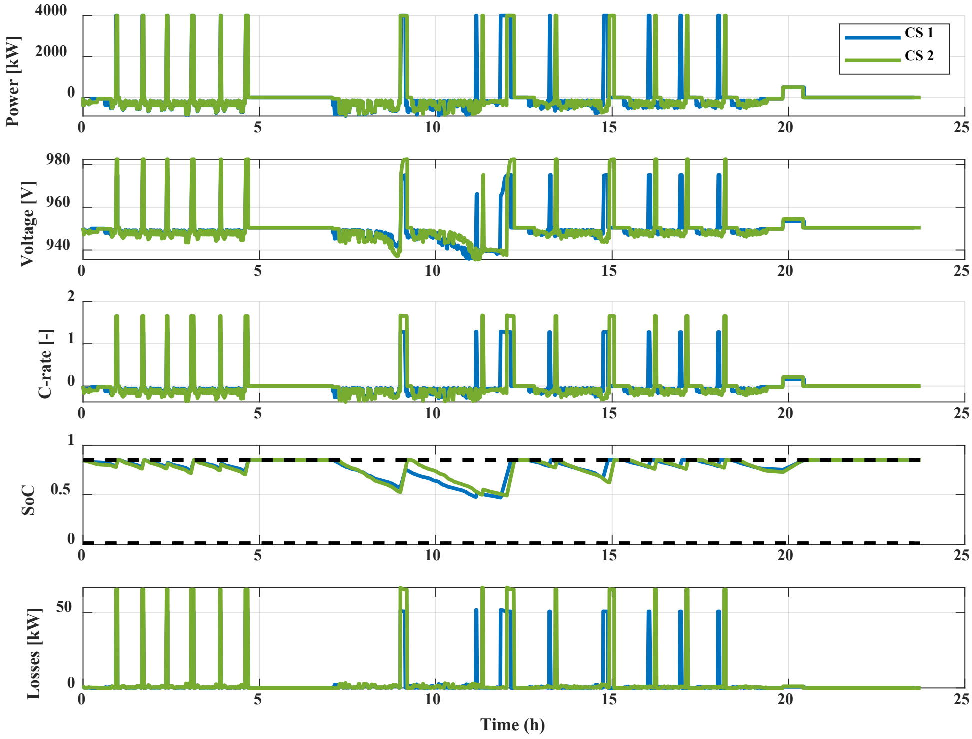

Figure 23. LFP-Mid battery operation for CS1, CS2, during the LCA use-phase operation.

The life cycle use-phase electric energy consumption for the battery electric ferry was determined as the energy taken from the grid, via an automatically connecting charger and grid-frequency transformer of 97% respectively 98% efficiency. The results are shown in *Table **10***.

Table 10. LCA use-phase energy consumption [MWh] for the two chemistries NMC and LFP and two charging scenarios CS1, CS2, during the LCA use-phase operation.

	NMC-1	NMC-2	LFP-1	LFP-2
For propulsion	-4.67	-4.51	-4.74	-4.56
From battery	4.84	4.75	4.86	4.71
From grid	5.10	5.00	5.12	4.95

Diesel engine propulsion

An engine efficiency map shown in *Figure **25***, was constructed after a few simplistic efficiency pointers for the engine (Penta, 2024). From the constructed efficiency map a fuel consumption map was derived. As a reference, a consumption map was also derived by interpolating the logged consumption. The deviation between the maps, reduces with increased power loading.

As another reference, data sheet stated fuel consumption along an exemplified propeller curve (Volvo Penta, 2021) is shown in Figure 24, as well as the resulting consumption for the same load using the constructed efficiency map and the one interpolated from the log. As noted in *Figure **15*** and *Figure **25***, all operating points occur above 1200 rpm. For this speed range, the constructed efficiency map overestimates the consumption by up to 2.5%, whereas the interpolated log underestimates the consumption by 2%-8%. A possible reason for the latter deviation could be diverging fuel material parameters. Here and in (Penta, 2021) the fuel mass density was 840 g/L and the lower heating value 42.7 MJ/kg.

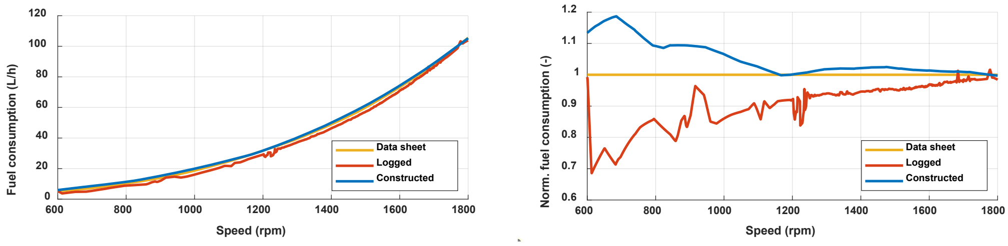

Figure 24. (Right) data sheet stated fuel consumption (yellow) along the exemplified propeller curve shown in ***Error! Reference source not found.****, vs. the consumption along the curve using the logged respective the constructed consumption maps. (Left) the same fuel consumption normalized with the data sheet graph.*

The operating points for the diesel propelled version of the ferry is shown in *Figure* ***25***, using the partly loaded diesel ferry weight. The resulting fuel consumption was **816.4 g**. Around 2540 Wh of propulsion power was used during the cruising mode and 1460 Wh during the various manoeuvring modes.

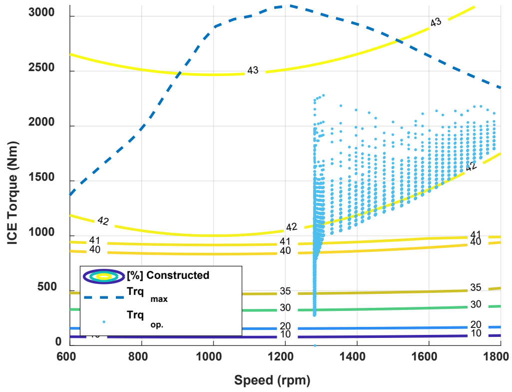

Figure 25. The diesel engine's constructed efficiency map, and its maximum torque line (Volvo Penta, 2021), along with LCA use-phase operating points, i.e. with the mass of a partly loaded ship.

Part 4 - Environmental assessment

The final part of the work was the environmental assessment using attributional LCA. This work has been divided into three sub-work packages, including the life cycle inventory analysis for the drive line, inventory analysis for the ferry's operation and environmental assessment. In this section, all three sections are jointly described. The inventories for the power train are analysed for the selected case study vessel and respective power train components as in Part 1 and Part 2 of the report. The operational data of the ferry is described in Part 1 under *Operational data*.

Goal and Scope

The goal is to compare the environmental impact of the different battery electric ferries (BEFs), bio-diesel-based ferries and fossil-diesel-based ferries over the entire life cycle. The BEFs chosen for comparison include a BEF fitted with LFP batteries and a BEF fitted with NMC622 batteries. In addition, two different charging strategies (as mentioned in Part 3 under "Final battery pack design, performance and charging") are compared for both types of BEFs to understand the impact of the charging strategy and battery dimension. By including these options, the analysis covers the variations in battery size, the impact of different charging strategies, the impact associated with the changes in the ship mass (different battery densities), and the impact associated with different lifetimes. In total six cases are compared:

1) BEF with an NMC622 battery pack with charging scenario 1 (BEFNMC1)

2) BEF with an NMC622 battery pack with charging scenario 2 (BEFNMC2)

3) BEF with an LFP battery pack with charging scenario 1 (BEFLFP1)

4) BEF with an LFP battery pack with charging scenario 2 (BEFLFP2)

5) ferry fueled by biodiesel (ICEFHVO)

6) ferry fueled by marine gas oil (ICEFMGO)

The functional unit of the study is the annual use of the ferry, and the system boundary consists of the life cycle of the ferry, including the shipbuilding, power train production, production of battery cells and packs, pack replacement, charging infrastructure, ferry operation, and electricity for charging. The system boundary is shown in *Figure 26*. For the data collection, the life cycle of the ferry has been divided into three parts (1) the ferry's life, including construction and manufacturing of the structure and drive line of the ferry, (2) Tank-to-wake (TTW), considering the ferry's operation, and (3) Well-to-tank (WTT), including electricity for charging and fuel production.

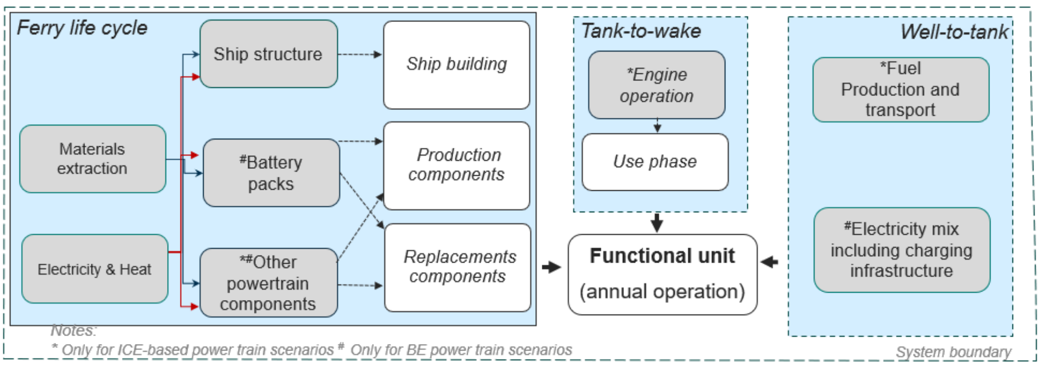

Figure 26. System boundary used in the study, including ferry life cycle, tank to wake, well-to-tank.

Inventory

Ferry life cycle: For the BEF, the most important component is the battery pack. The battery packs contain except for the battery cells, module, and pack components. The inventory data used for the battery cells is from the battery-design model described in Part 2 (Battery modeling) and the material inventories for the cell components (electrodes, current collectors, container, electrolyte, etc.) are based on data from previous studies (Chordia et al., 2021, Ager-Wick Ellingsen et al., 2022, Dai et al., 2019, Sun et al., 2020, Shu et al., 2021, Degen and Schütte, 2022, Degen et al., 2023, Jiang et al., 2023). The battery module, thermal management system, electrical system, and battery pack components are sized for the case study, and the inventory is based on previous studies (Ellingsen et al., 2014, Ellingsen et al., 2023, Dai et al., 2019).

For BEFs, other important power train components are the inverter and the electric motor. The detail of the electric motor used in this study is mentioned in Part 2, while the data for the material inventory and production processes are derived from previous studies (Nordelöf et al., 2017, Nordelöf and Tillman, 2017). The assumption is that the inverter model is modular and that the inventory can be estimated linearly using data from a previous LCA study (Nordelöf et al., 2018). The inventory for the marine engines and the auxiliary engines is based on generic data based on previous studies (Kanchiralla et al., 2023, Kanchiralla et al., 2022). The ship structure used is based on (Light Dead weight Tonnage) LDT and also based on generic data from previous studies. The boiler and the heat pump inventories are adopted from previous study (Kanchiralla et al., 2024).

Components like the battery pack have a lower service life than the lifetime of the ferry (40 years). For ICE options, the engines are assumed to need to be replaced after 20 years. Battery replacements are assumed based on the battery type, depth of discharge (DoD), and cycles. Given the design parameters and operations, the battery life is calculated based on the degradation model suggested in a previous study (Olmos et al., 2021). According to the calculation, the NMC battery needs to be replaced more frequently than the LFP, and the replacement frequency during 40 years of ferry operation is given in *Table **11***. The materials considered to produce the above components are assumed from the Ecoinvent 3.9 database and geographical location is assumed in Europe. The end-of-life modeling is based on the cut-off approach, considering the recycled material shares as input to raw material production upstream.

Table 11: The number of replacements and life of battery calculated for BEF scenarios.

		NMC1	NMC2	LFP1	LFP2
Battery pack replacement	*number*	2	3	2	2
Equivalent cycles per year	*number*	522	710	562	706
Life of battery	years	13	10	15	13

Well-to-tank: The Swedish electricity mix is considered for charging the batteries during the use phase and the ferry is assumed to be operating in the future. A prospective Swedish electricity mix based on the SSP2 NDC scenario modeled in premise is used (Sacchi et al., 2022), where the electricity mix from 2025 to 2065 is considered for charging during ferry operation. The same approach is used in biodiesel production. The biodiesel considered in this study is hydrogenated vegetable oil (HVO). The biological feedstock used in the HVO is assumed to be based on the present Swedish mix of HVO production, where 76% comes from animal fats, 12% from used cooking oil, and the rest from different vegetable oils. The data for the HVO production is from Edwards et al. (2019). The fossil diesel production is taken from Ecoinvent 3.9.

Tank-to-wake: The assumed TTW emissions for the BEFs are zero. The fuel consumption and emissions of ICEFs are influenced by the engine load. In this study, a simplified assumption is made by considering the load based on the speed of the ship. At speeds below 8 knots and when pushing against dock, the emissions profile based on an engine load of 20% is considered. When the speed exceeds 8 knots, the emission profile for engine load 70% is assumed. In addition to the emission from the engines, there is emission from the boiler, which is calculated based on the seasons. The emission factors for the diesel are considered based on different studies (International Maritime Organization, 2021, Kanchiralla et al., 2023), and emission from the boiler is considered from IMO fourth GHG study (International Maritime Organization, 2021, Kanchiralla et al., 2024). The CO_2 from the HVO combustion (engine and boiler) is assumed as biogenic. More information about the method and inventory used for the environmental assessment can be found in the manuscript under preparation (Kanchiralla et al.).

Impact assessment

This study evaluates the environmental effects across seven specific impact categories: global warming potential (GWP), particulate matter formation potential (PM), terrestrial acidification potential (AP), marine eutrophication potential, ozone depletion potential (ODP), freshwater ecotoxicity potential (FEP), surplus ore potential (SOP) and critical scarcity indicator (CSI). The calculation of GWP is determined by utilizing a 100-year timeframe and employing the characterization factor found in the IPCC AR6. (IPCC, 2022), CSI is estimated using the crustal scarcity indicator characterization method (Arvidsson et al., 2020). The ReCiPe 2016 v1.03 midpoint (Heirarchist view) was used to estimate all other impact categories (Huijbregts et al., 2016).

Life cycle assessment results

Figure 27 presents the cradle-to-grave GWP for the annual use of the ferry for the selected six cases. All BEF options have more than 90% lower GWP than the equivalent diesel-electric option using MGO. The major emission for the diesel option is emission during TTW when the diesel is burned. The TTW emissions of HVO are low as the CO_2 emission is considered biogenic, however, there are some impacts associated with the use of urea as a consumable for selective catalytic reduction (SCR) (NOx abatement). For both BEFs and all scenarios, the well-to-tank (WTT) phase has the highest contribution, i.e. emissions caused by electricity generation, followed by the impact associated with the production of the battery packs (initial acquisition and replacement). Compared to the first scenario second scenario has 3.5% times lesser climate impact in case of NMC. For LFP, the second scenario has 8.5% lesser climate impact than first scenario. This indicates that the lower energy consumption due to lower weight and lower installed capacity offsets the impact of a higher number of replacements. Compared to previous studies (Perčić et al., 2022, Guven and Ozgur Kayalica, 2023), the case study's climate impact is relatively low, and this is mainly associated with the electricity mix used for charging. The Swedish electricity mix is considered in the study for which the carbon intensity is low (28 gCO_{2eq}/kWh).

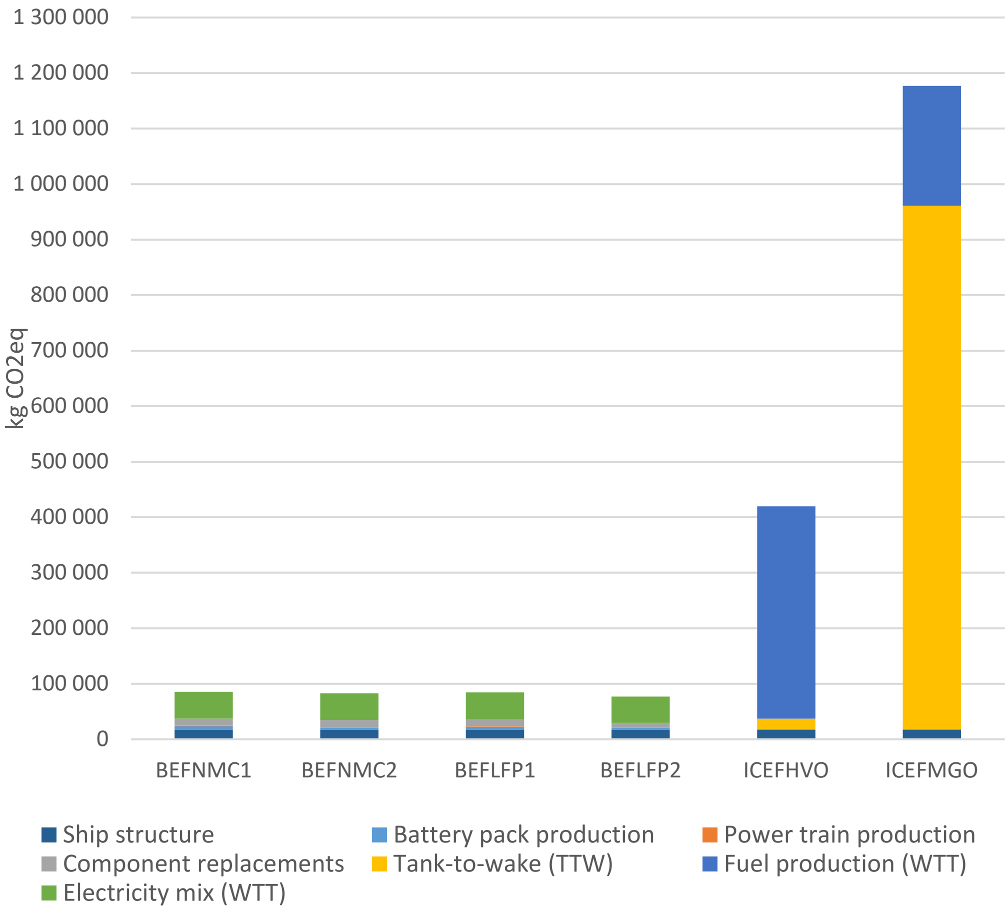

Figure 27. Annual global warming potential in a hundred-year time horizon (GWP100) in kg CO_2 equivalents for the BEF cases investigated including conventional ICE options using hydrotreated vegetable oil (ICEFHVO) and marine gas oil (ICEFMGO).

Figure 28 (a) shows the comparison between the two different battery types (NMC622 and LFP) for 1 kWh battery produced from cradle-to-gate. In *Figure 28* (b) it is shown that the NMC alternative has higher emissions than the LFP alternative, and the difference in weight affects less than the differences related to the emissions caused by battery production and their replacements. This is mainly due to the higher number of replacements required for NMC batteries (due to their shorter cycle-life) as well as the higher impact associated with NMC battery production. The higher impact for NMC batteries is the higher emissions associated with the NMC cathode production compared to the LFP cathode production. This can also be observed in the other inventory datasets like GREET (Dai et al., 2019).

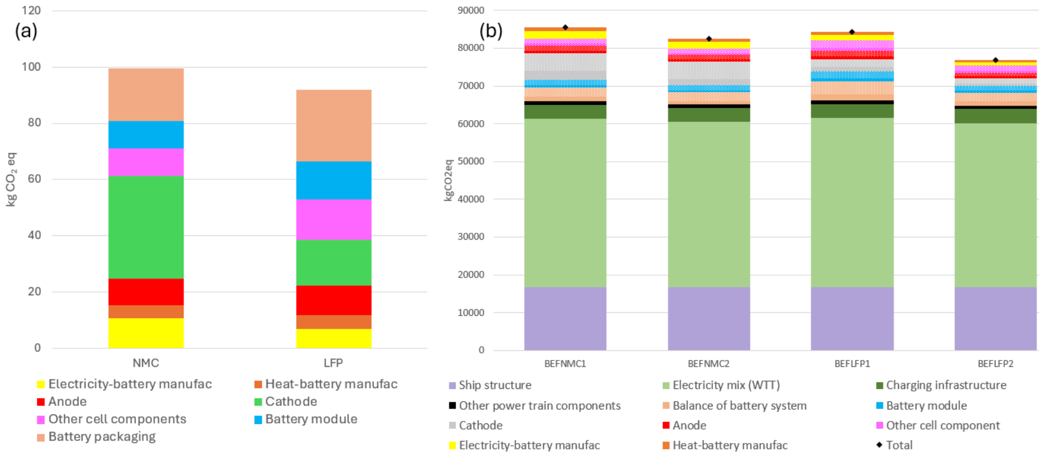

Figure 28. (a) Breakdown of the global warming potential connected to battery production for the mid-optimized NMC and LFP batteries in kg CO_2 equivalents for 1 kWh battery. (b) Annual global warming potential in a hundred-year time horizon (GWP100) in kg CO_2 equivalents for the two battery chemistries under two different charging scenarios with break-down of the battery production.

Figure 29 compares eight impact categories mentioned in section impact assessment for the six selected cases. BEF options have lower ozone depletion, particulate matter, marine eutrophication, and acidification potential impacts compared to both biodiesel and fossil diesel. The above impacts are affected mainly by the emission of PM2.5, SOx, NOx, and other air emissions during the operation phase (Tank to wake). However, surplus ore potential and freshwater ecotoxicity are significantly higher for the BEF cases which can be linked with the critical material and minerals required for both the production of batteries as well as for electricity generation (infrastructure). Detailed results are available in the manuscript under preparation (Kanchiralla et al.).

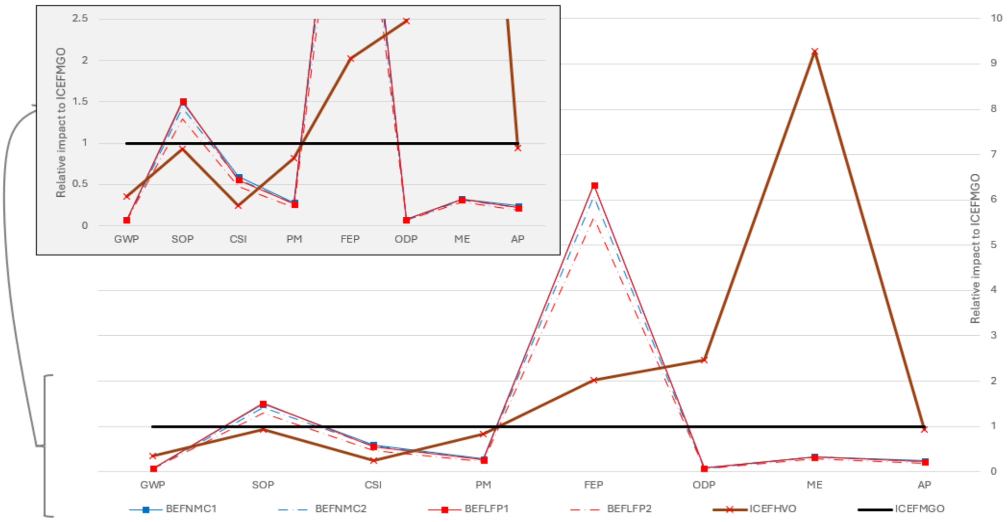

Figure 29. Comparison of different impact categories for the investigated cases normalized to the annual potential impact of the ferry using MGO. GWP: global warming potential, PM: particulate matter formation potential, AP: terrestrial acidification potential, ME: marine eutrophication potential, ODP: ozone depletion potential, FEP: freshwater ecotoxicity potential, SOP: surplus ore potential, and CSI: critical scarcity indicator.

Energimyndigheten

Discussion

The overall aim of this study was to further build the necessary knowledge of factors that could reduce the environmental impact of marine transport with current and future technology solutions. As preferred solutions may differ depending on type of ship and service provided, both fleet-level and more detailed single ship-level studies will give vital insights. This study falls in the latter category.

The specific project goal was to, for a ship operating in Swedish waters, determine the proportions of the environmental burden that falls on a diesel driven ship as opposed to a battery electric version of the same ship, as well as establishing the contributions due to the various subparts such as battery, drive system components and the ship itself. The investigated propulsion solutions comprised electric motors with and without magnets, an inverter unit and batteries of two different chemistries (LFP, NMC), which were optimized for energy respective power, as well as a middle of the two (in total six different cells). A further aim was to base the environmental analysis on ship-specific hull, propeller and propulsion system components with load dependent models of energy and fuel consumption.

The selected ship to study was a passenger ferry operating between mainland and islands in Gothenburg's southern archipelago, as well as on the river Göta älv, in a rather complex pattern. The electric drive system dimensioning and environmental impact assessment was based on logged operation data which strengthens the relevance of the study, as well as on assumptions regarding possible charging places and power levels.

Battery packs of six different cell designs, all with different strengths and weaknesses, were dimensioned to meet the ferry's operating requirements. As was expected, the energy density of the NMC-based packs was higher compared to the LFP packs. To fully utilize the strength of the power-optimised cells, and to some extent also the Mid-optimized cells, charging power levels above what is so far commercialized would be needed. To fulfil the energy demand with a believed realistic charging power the packs thus became rather heavy. For the packs with the energy optimized cells, the charging power limit was even lower, but compensated somewhat due to their higher energy density. Still, the lightest packs were achieved with the Mid designed cells, which provided both high energy density and fast charging capability. Furthermore, a route modification was exemplified as prolonged stop time for charging at a critical point of the day, and the consequence on battery capacity, ship weight and LCA results were quantified. The exemplified charging time modification led to significant reductions (33%) in the required installed battery capacity onboard.

The study shows that a battery electric version of the chosen ship could significantly lower the **climate impact** over the ferry's lifetime, compared to the two studied combustion engine alternatives, even when considering battery pack replacements. Already within one year of operation, both the fossil fuel powered, and the bio-diesel ferry versions overtake the battery-electric ferry (BEF) regarding climate impact. When comparing the two battery chemistries, LFP has a lower impact than NMC even though the LFP-ship's energy use was higher due to a higher ship mass. The advantage is mainly due to the higher cycle life offered by the LFP compared to the NMC for the selected Depth of Discharge (DoD)[5] as well as to the lower impact of cathode production. Still, the highest contribution for the BEF was associated with electricity use in the well-to-tank phase, which highlights a continued need to decrease climate impact of electricity production.

In addition to the potential to reduce the climate impact, the battery electric ferry versions have lower **ozone depletion**, **particulate matter**, **marine eutrophication**, and **acidification potential** impacts than the combustion engine versions, mainly linked to the zero-emission operation. In contrast, **resource scarcity** and the impact on **ecotoxicity** due to higher requirements of minerals like copper, lithium, cobalt, nickel, zinc, and rare earth metals would be environmental challenges for the BEF cases.

Even though the contribution to the ferry's climate impact due to the electric motors and inverters was rather low, in a possible increased degree of electrification, it would be interesting to further investigate various machine types and system configurations. For instance, using a dc-dc converter on the dc-bus could potentially reduce the required mass of the electric machines. Moreover, a deeper technical analysis on the interplay between charging solutions and power ratings on the one hand, and battery chemistry, configuration and lifetime on the other, would generally be a highly valuable input to this kind of environmental assessment of marine transport, both on shorter and longer operating routes.

This project offered a great opportunity to develop detailed insights into how marine propulsion systems and its components could be dimensioned, configured and modelled. Furthermore, the interdisciplinary collaboration at Chalmers and with related industry are both deepened and widened.

[5] DOD is here equivalent to the stated "reached SoC_{min}" in Part 2 of the report.

Publication list

The project has resulted in the following publications:

Kanchiralla, F. M., Brynolf, S., Grunditz, E., Wikner, E., Nordelöf, A., Economic and Environmental Footprints of Electric Ferries: A Life Cycle Analysis of Lithium-Ion Battery Technologies. Manuscript to be submitted for scientific journal.

Grunditz, E., Wikner, E., Kanchiralla, F. M., Brynolf, S., Electric drivetrain and battery sizing for a battery electric passenger ferry operating in Sweden. Manuscript to be submitted for scientific journal.

Wikner, E., Lacey, M., A flexible battery cell design and composition model. Manuscript to be submitted for scientific journal.

Methods and results from the project have been and will be presented at the following conference events:

Wikner, E., Lacey, M., Chordia, M., Nordelöf, A., Thiringer, T., A model platform for life cycle assessment of lithium-ion battery production and use, Nordbatt 2022, Gothenburg, Sweden.

Kanchiralla, F. M., Brynolf, S., Grunditz, E., Wikner, E., Nordelöf, A, Life Cycle Assessment of Electric Ferries Based on Various Lithium-ion Battery Technologies. Extended abstract accepted for poster presentation at SETAC Europe 26th LCA Symposium, 21 – 23 October 2024, Gothenburg, Sweden

References

AGER-WICK ELLINGSEN, L., JAYNE THORNE, R., WIND, J., FIGENBAUM, E., ROMARE, M. & NORDELÖF, A. 2022. Life cycle assessment of battery electric buses. *Transportation Research Part D: Transport and Environment,* 112.

ALDRIDGE, I. N. B. A. M. F. 2019. Power models and average ship parameter effects on marine emissions inventories. *Journal of the Air & Waste Management Association,* 69**,** 752-763.

ARFA GRUNDITZ, E. & THIRINGER, T. Electric Vehicle IGBT Power Module Sizing and Drive Cycle Energy Efficiency for Various Switching Frequencies-Based on a Scalable Module Model. 2018 Riga, Latvia. 20th European Conference on Power Electronics and Applications (EPE'18 ECCE Europe).

ARVIDSSON, R., SÖDERMAN, M. L., SANDÉN, B. A., NORDELÖF, A., ANDRÉ, H. & TILLMAN, A.-M. 2020. A crustal scarcity indicator for long-term global elemental resource assessment in LCA. *The International Journal of Life Cycle Assessment,* 25**,** 1805-1817.

BERG PROPULSION 2022-2024. Personal communication, Engineering Manager, Tobias Huuva. Gothenburg.

CARLTON, J. C. 2007. *Marine Propellers and Propulsion,* Oxford, Butterworth-Heinemann, Elsevier Ltd.

CAVOTECH 2024. Shore power. *solutions for ships.*
CHORDIA, M., NORDELÖF, A. & ELLINGSEN, L. A.-W. 2021. Environmental life cycle implications of upscaling lithium-ion battery production. *The International Journal of Life Cycle Assessment*.
CHORDIA, M., WIKNER, E. & NORDELÖF, A. 2022. A model platform for solving lithium-ion battery cell data gaps in life cycle assessment. *EVS35 Symposium.* Oslo, Norway.
DAI, Q., KELLY, J. C., GAINES, L. & WANG, M. 2019. Life Cycle Analysis of Lithium-Ion Batteries for Automotive Applications. *Batteries,* 5.
DANFOSS 2022. Ellen,the world's longest ranging electric ferry. IEA's 7th Annual Global Conference on Energy Efficiency.
DEGEN, F. & SCHÜTTE, M. 2022. Life cycle assessment of the energy consumption and GHG emissions of state-of-the-art automotive battery cell production. *Journal of Cleaner Production,* 330.
DEGEN, F., WINTER, M., BENDIG, D. & TÜBKE, J. 2023. Energy consumption of current and future production of lithium-ion and post lithium-ion battery cells. *Nature Energy,* 8**,** 1284-1295.
DNV GL AS MARITIME. 2020. Study on electrical energy storage for ships-Battery systems for maritime applications – technology, sustainability and safety. EMSA.
EDWARDS, R., O'CONNELL, A., PADELLA, M., GIUNTOLI, J., KOEBLE, R., BULGHERONI, C., MARELLI, L. & LONZA, L. 2019. Definition of input data to assess GHG default emissions from biofuels in EU legislation, Version 1d. Luxembourg.
ELLINGSEN, L. A.-W., MAJEAU-BETTEZ, G., SINGH, B., SRIVASTAVA, A. K., VALØEN, L. O. & STRØMMAN, A. H. 2014. Life Cycle Assessment of a Lithium-Ion Battery Vehicle Pack. *Journal of Industrial Ecology,* 18**,** 113-124.
ELLINGSEN, L. A.-W., THORNE, R. J., WIND, J., FIGENBAUM, E., ROMARE, M. & NORDELÖF, A. 2023. Corrigendum to "Life cycle assessment of battery electric buses" [Transp. Res. Part D: Transp. Environ. 112 (2022) 103498]. *Transportation Research Part D: Transport and Environment,* 116.
GUVEN, D. & OZGUR KAYALICA, M. 2023. Life-cycle assessment and life-cycle cost assessment of lithium-ion batteries for passenger ferry. *Transportation Research Part D: Transport and Environment,* 115.
HETTESHEIMER, T., NEEF, C., INCLÁN, R., LINK, S., SCHMALTZ, T., SCHUCKERT, F., STEPHAN, A., STEPHAN, M., THIELMANN, A., WEYMANN, L. & WICKE, T. 2023. Lithium-Ion Battery Roadmap – Industrialization Perspectives Toward 2030. Karlsruhe, Germany: Fraunhofer Institute for Systems and Innovation Research ISI.
HOEDEMAKER, S. T. C. 2023. Current Status of Maritime Batteries and Future Outlook. Rotterdam, Netherlands: Maritime Battery Forum.
HOLTROP, J. 1984. A statistical re-analysis of resistance and propulsion data. *International Shipbuilding Progress, ISP,* 31**,** 272-276.
HOLTROP, J. & MENNEN, G. G. J. 1982. An approximate power prediction method. *International Shipbuilding Progress, ISP,* 29.

HUIJBREGTS, M. A. J., STEINMANN, Z. J. N., ELSHOUT, P. M. F., STAM, G., VERONES, F., VIEIRA, M. D. M., HOLLANDER, A., ZIJP, M. & VAN ZELM, R. 2016. ReCiPe 2016 A harmonized life cycle impact assessment method at midpoint and endpoint level Report I: Characterization. Bilthoven, The Netherlands: National Institute for Public Health and the Environment.

INFINEON 2024. FF900R17ME7W_B11, EconoDUAL™3 module, Final datasheet. Munich: Infineon Technologies AG.

INTERNATIONAL MARITIME ORGANIZATION 2021. Reduction of GHG emissions from Ships: Fourth IMO GHG Study 2020. London: International Maritime Organization.

IPCC 2022. Assessment report 6: Climate Change 2022: Mitigation of Climate Change.

JIANG, T., WANG, H. & JIN, Q. 2023. Comparison of three typical lithium-ion batteries for pure electric vehicles from the perspective of life cycle assessment. *Clean Technologies and Environmental Policy,* 26**,** 331-350.

KANCHIRALLA, F. M., BRYNOLF, S., MALMGREN, E., HANSSON, J. & GRAHN, M. 2022. Life-Cycle Assessment and Costing of Fuels and Propulsion Systems in Future Fossil-Free Shipping. *Environ Sci Technol,* 56**,** 12517-12531.

KANCHIRALLA, F. M., BRYNOLF, S., OLSSON, T., ELLIS, J., HANSSON, J. & GRAHN, M. 2023. How do variations in ship operation impact the techno-economic feasibility and environmental performance of fossil-free fuels? A life cycle study. *Applied Energy,* 350.

KANCHIRALLA, F. M., BRYNOLF, S. & REIS DE OLIVEIRA, D. S. 2024. Heat Pump as an Emission Reduction Measure for Ships. *Modelling and Optimisation of Ship Energy Systems 2023*.

KIM, Y.-R., STEEN, S., KRAMEL, D., MURI, H. & STRØMMAN, A. H. 2023. Modelling of ship resistance and power consumption for the global fleet: The MariTEAM model. *Ocean Engineering,* 281**,** 114758.

MAN 2023. Basic principles of ship propulsion. Denmark: MAN Energy Solutions.

MEPC. 2023. *Marine Environment Protection Committee (MEPC)* [Online]. IMO. Available: https://www.imo.org/en/MediaCentre/MeetingSummaries/Pages/MEPC-default.aspx [Accessed 10 Jul 2023].

NORDELÖF, A., ALATALO, M. & SÖDERMAN, M. L. 2018. A scalable life cycle inventory of an automotive power electronic inverter unit—part I: design and composition. *The International Journal of Life Cycle Assessment,* 24**,** 78-92.

NORDELÖF, A., GRUNDITZ, E., TILLMAN, A.-M., THIRINGER, T. & ALATALO, M. 2017. A scalable life cycle inventory of an electrical automotive traction machine—Part I: design and composition. *The International Journal of Life Cycle Assessment,* 23**,** 55-69.

NORDELÖF, A. & TILLMAN, A.-M. 2017. A scalable life cycle inventory of an electrical automotive traction machine—Part II: manufacturing processes. *The International Journal of Life Cycle Assessment,* 23**,** 295-313.

OLMOS, J., GANDIAGA, I., SAEZ-DE-IBARRA, A., LARREA, X., NIEVA, T. & AIZPURU, I. 2021. Modelling the cycling degradation of Li-ion batteries: Chemistry influenced stress factors. *Journal of Energy Storage,* 40.

PENTA, V. 2024. Personal communication. Gothenburg.

PERČIĆ, M., FRKOVIĆ, L., PUKŠEC, T., ĆOSIĆ, B., LI, O. L. & VLADIMIR, N. 2022. Life-cycle assessment and life-cycle cost assessment of power batteries for all-electric vessels for short-sea navigation. *Energy,* 251.

SACCHI, R., TERLOUW, T., SIALA, K., DIRNAICHNER, A., BAUER, C., COX, B., MUTEL, C., DAIOGLOU, V. & LUDERER, G. 2022. PRospective EnvironMental Impact asSEment (premise): A streamlined approach to producing databases for prospective life cycle assessment using integrated assessment models. *Renewable and Sustainable Energy Reviews,* 160.

SHU, X., GUO, Y., YANG, W., WEI, K. & ZHU, G. 2021. Life-cycle assessment of the environmental impact of the batteries used in pure electric passenger cars. *Energy Reports,* 7**,** 2302-2315.

STEMMANN-TECHNIK 2024. FerryCHARGER. *charging solutions for electric ferries.*

STYRSÖBOLAGET 2022. Personal communication, Technology Manager, Mats Börjesson. Gothenburg.

STYRSÖBOLAGET 2023. Om oss, Fartyg, Vesta.

STÄUBLI 2024. Electrical Connections. *QCC connection solutions for e-mobility.*

SUN, X., LUO, X., ZHANG, Z., MENG, F. & YANG, J. 2020. Life cycle assessment of lithium nickel cobalt manganese oxide (NCM) batteries for electric passenger vehicles. *Journal of Cleaner Production,* 273.

VESTA 2024. visit onboard.

VOLVO PENTA. 2021. Inboard Diesel. *D16-MH, data sheet* [Online]. Available: https://pubs.volvopenta.com/publications//47713991 [Accessed January 2021].

ZINUS 2024. Charging telescopic autonomous.

Appendix A - Overview of fully electric ferries

The data was collected in the early 2022, hence possible later updates are not included.

Table 12. Overview of fully electric ferries early 2022; part 1 of 4.

	Ship name	Country of operation	Rute City	Rute distance (km)	Rute duration (min)	Frequency of operation
1	Movia	DK	Copenhagen			
2	M/F Tyco Brahe, M/F Aurora	DK-SE	Helsingborg-Helsingör	5	20	every 15min, 24h/day
3	Ellen	DK	Søby - Fynshav	2x20	60	5-7 times/day
4	Föri	FI	Aura river	0.5	2	400 times/day
5	Ar Vag Tredan	FR	Lorient-Locmiquélic		7	28 times /day
6	Sankta Maria	DE-LU	Wasserbillig-Oberbillig			
7	El ferry from Iceland	IS	Landeyjahöfn-Westman Island	13	45	
8	M F Ampere	NO	Larvik-Oppedal	5.7	20	34 times/day
9	Future of the Fjords	NO	Gudvangen-Flåm			5 times/day
10	Byferga	NO	Gamblebyen-Gressvik, Fredrkstad city		15	6 times/h
11	Boreal	NO	Kvanndal-Utne		28	
12	E/S Movitz	SE	Solna Strand - Stockholm's Old Town	10	70	4 times/day
13	MS Sjövägen	SE	Frihamnen-Nybrokajen, Stockholm			8 times/day
14	MariArt Ferry	TH	Hua Lampjong-Thewes Pier	5		
15	Excursion Ferry					
16	Amherst island ferry	CA	Amherst			
17	Wolfe island ferry	CA	Wolfe island,			
18	Grotte	DK	Esbjerg-Island Fanö			
19	Junlu	CN	Yangtze River, Wuhan			
20	Aditya	IN				
21	Zhongtiandianyun 001	CN				
22	Stena Elektra (2030)	SE-DK	Göteborg-Fredrikshamn			
23	Bastø Electric	NO	Oslo Fjord, Moss-Horten	10	30	20-24 times/day
24	MF Gloppefjord, Eidsfjord	NO	Anda-Lote	2	8	
25	MM82FE EL	NO	Ranavik-Skjersholmane	14		
26	new (2019)	NO	Gjermundshamn-Årsnes			
27	MM111FE EL	NO	Jondal-Tørvikbygd			
28	MM70FE EL	NO	Kvanndal-Utne			
29	MF Husavik (2018)	NO	Husavik-Sandvikvåg	6.8	20	
30	Kaohsiung	TW	Kaohsiung			
31	E-Oshima (2019)	JP				

Table 13. Overview of fully electric ferries early 2022; part 2 of 4.

	Ship name	Passen-gers	Cars	Trucks	Length (m)	Width (m)	Max speed (knots)
1	Movia	80			23	5.6	
2	M/F Tyco Brahe, M/F Aurora	1250	240		111		14
3	Ellen	198	31	5	60	13	13-15.5
4	Föri	75					
5	Ar Vag Tredan	150			22.1	7.2	10
6	Sankta Maria	45	6		28	7.9	
7	El ferry from Iceland	550	75		70		
8	M F Ampere	360	120		80	20	
9	Future of the Fjords	400			42.5	15.2	16
10	Byferga	50			15		10
11	Boreal	199	60		75	14.2	
12	E/S Movitz	100			23		9
13	MS Sjövägen				24.5		8.5
14	MariArt Ferry	40					
15	Excursion Ferry						
16	Amherst island ferry	300	42		68	25	12
17	Wolfe island ferry	399	75		98	25	12
18	Grotte				50	14	11
19	Junlu	300			53	13	10
20	Aditya	75			21		7.5
21	Zhongtiandianyun 001				70		7
22	Stena Elektra (2030)	1500	700	160	250		
23	Bastø Electric	600	200		139	21	13
24	MF Gloppefjord, Eidsfjord	349	120	12	106		
25	MM82FE EL	299	83		85		13
26	new (2019)						
27	MM111FE EL	299	130				
28	MM70FE EL	199	60		75		
29	MF Husavik (2018)	199	45		64	14.4	
30	Kaohsiung	150			25		9
31	E-Oshima (2019)						

Table 14. Overview of fully electric ferries early 2022; part 3 of 4.

	Ship name	EM Manufacturer, type	No EMs	EM power (MW)	Battery Manu-facturer	Battery energy capacity (kWh)
1	Movia		2	0.055		120
2	M/F Tyco Brahe, M/F Aurora	Azimuth thruster	2	1.5	XALT Energy	4160
3	Ellen	Danfoss, propulsion, thruster, PMaSRM	4	1.5	Leclanché	4300
4	Föri	Danfoss	2		Corvus/ LG chem	57
5	Ar Vag Tredan	Azimuth thruster			Bolloré, Blue Solution	
6	Sankta Maria				EST floattech/ Kokam	10.5
7	El ferry from Iceland	ABB			ABB	3000
8	M F Ampere	Siemens	2	1.8	Corvus	1090
9	Future of the Fjords	Westcon Power and Automation, PM	2	0.9	Akasol / SAMSUNG	1800
10	Byferga	Danfoss		0.15	Akasol / SAMSUNG	100
11	Boreal					
12	E/S Movitz	Echandia Marine		0.25	Nilar	180
13	MS Sjövägen				SAFT	500
14	MariArt Ferry	Torqeedo	2	0.2		
15	Excursion Ferry					
16	Amherst island ferry					
17	Wolfe island ferry					
18	Grotte	Danfoss	2	0.75		1107
19	Junlu					
20	Aditya					50
21	Zhongtiandianyun 001					2400
22	Stena Elektra (2030)					70000
23	Bastø Electric					4300
24	MF Gloppefjord, Eidsfjord				PBES	180
25	MM82FE EL					
26	new (2019)					
27	MM111FE EL					
28	MM70FE EL					
29	MF Husavik (2018)				Corvus Orca Energy	1590
30	Kaohsiung					

31	E-Oshima (2019)	CS Yuasa	600

Table 15. Overview of fully electric ferries early 2022; part 4 of 4.

	Ship name	Charging solution	Charging power (MW)	Charging time (min)
1	Movia	Automated at endpoints		
2	M/F Tyco Brahe, M/F Aurora	Fully automatic ABB laser-controlled robot arm	11.2, 10.35	Helsingör 5min30s , Helsingborg 9min
3	Ellen	Mobimar designed automatic charging arms	4	Docked: 20min, night
4	Föri	Over night		
5	Ar Vag Tredan			4
6	Sankta Maria			360
7	El ferry from Iceland	In both harbours	2.5	30
8	M F Ampere	410 kWh battery at each dock for charging		10
9	Future of the Fjords	Westcon power and automation	1.2	20
10	Byferga	Inductiive charging by IPT Technology	0.1	112s, ca 2min 2kWh
11	Boreal			
12	E/S Movitz		0.3	10
13	MS Sjövägen			
14	MariArt Ferry			
15	Excursion Ferry			
16	Amherst island ferry			
17	Wolfe island ferry			
18	Grotte		2.6	7
19	Junlu			
20	Aditya			
21	Zhongtiandianyun 001			
22	Stena Elektra (2030)			
23	Bastø Electric		9	
24	MF Gloppefjord, Eidsfjord			
25	MM82FE EL		5	
26	new (2019)			
27	MM111FE EL			
28	MM70FE EL			
29	MF Husavik (2018)			
30	Kaohsiung			
31	E-Oshima (2019)			150

Appendix B – Battery cell specifications

In this section the complete cell component mass breakdown from the cell design model is included in Table 16 for the NMC cells and in Table 17 for the LFP cells.

The data used of the performance model in COMSOL is included in Table 18 and Table 19. The material parameters were taken from COMSOLs inbuilt material library.

Table 16. NMC cell material and weight distribution per component [g].

Component	Power Optimised	Mid Optimised	Energy Optimised
Positive electrode – NMC622	**778.3**	**824.9**	**787.6**
Positive electrode paste (active)	*590.6*	*724.3*	*714.5*
Carbon black and Binder	*24.6*	*30.2*	*29.8*
Positive electrode current collector (foil)	*159.2*	*66.6*	*39.4*
Positive tab compensation (foil)	*3.9*	*3.9*	*3.9*
Negative electrode – Graphite	**875.4**	**717.6**	**655.0**
Negative electrode paste (active)	*380.5*	*485.1*	*500.2*
Carbon black and Binder	*11.8*	*15.0*	*15.5*
Negative electrode current collector (foil)	*470.1*	*204.5*	*126.5*
Negative tab compensation (foil)	*12.9*	*12.9*	*12.9*
Electrolyte	**177.0**	**217.1**	**214.2**
Separator	**181.4**	**83.1**	**54.2**
Cell container assembly	**271.5**	**271.5**	**271.5**
Cylindrical casing	*166.4*	*166.4*	*166.4*
Lid	*90.0*	*90.0*	*90.0*
Fastening tape	*0.0*	*0.0*	*0.0*
Insulation ring	*15.0*	*15.0*	*15.0*
Total	**2283.5**	**2114.2**	**1982.5**

Table 17. LFP cell material and weight distribution per component [g]

Component	Power Optimised	Mid Optimised	Energy Optimised
Positive electrode – LFP	**749.5**	**765.3**	**712.3**
Positive electrode paste (active)	*581.7*	*678.8*	*650.1*
Carbon black and Binder	*24.2*	*28.3*	*27.1*
Positive electrode current collector (foil)	*139.7*	*54.3*	*31.2*
Positive tab compensation (foil)	*3.9*	*3.9*	*3.9*
Negative electrode – Graphite	**764.7**	**596.2**	**535.5**
Negative electrode paste (active)	*327.5*	*401.6*	*407.1*
Carbon black and Binder	*10.1*	*12.4*	*12.6*
Negative electrode current collector (foil)	*414.2*	*169.3*	*103.0*
Negative tab compensation (foil)	*12.9*	*12.9*	*12.9*
Electrolyte	**151.7**	**177.1**	**169.6**
Separator	**160.7**	**70.1**	**45.5**
Cell container assembly	**271.5**	**271.5**	**271.5**
Cylindrical casing	*166.4*	*166.4*	*166.4*
Lid	*90.0*	*90.0*	*90.0*
Fastening tape	*0.0*	*0.0*	*0.0*
Insulation ring	*15.0*	*15.0*	*15.0*
Total	**2098.1**	**1880.1**	**1734.5**

Table 18. Cell component NMC622 vs. graphite

Component NMC622 vs Graphite	Power optimsed	Mid optimsed	Energy optimsed
Positive electrode area (m^2)	9.7	4.1	2.4
Positive electrode current collector area (m^2)	4.9	2.1	1.2
Positive electrode thickness (µm)	20.0	58.6	97.7
Positive electrode volume fraction	0.6	0.6	0.6
Positive electrode current collector (foil) (µm)	12.0	12.0	12.0
Positive electrolyte volume fraction	0.4	0.4	0.4
Positive electrode additive volume faction	0.1	0.1	0.1
Positive particle diameter (µm)	10.0	10.0	10.0
Negative electrode area (m^2)	10.4	4.5	2.8
Negative electrode current collector area (m^2)	5.2	2.3	1.4
Negative electrode thickness (µm)	25.9	75.9	126.6
Negative electrode volume fraction	0.6	0.6	0.6
Negative electrode current collector (foil) (µm)	10.0	10.0	10.0
Negative electrolyte volume fraction	0.4	0.4	0.4
Negative electrode additive volume fraction	0.0	0.0	0.0
Negative particle diameter (µm)	10.0	10.0	10.0
Separator thickness (µm)	16.0	16.0	16.0
Separator porosity	0.4	0.4	0.4
Areal capacity (mA/cm^2)	1.0	3.0	5.0
Simulated capacity 3.65-2.5 V (Ah) @0.1C	101.8	124.9	123.2
Simulated energy 3.65-2.5 V (Wh) @0.1C	373.0	457.1	450.5
Calculated Cell capacity (Ah)	99.7	122.2	120.6
Calculated Cell energy (Wh)	363.8	446.1	440.1
Calculated energy density (Wh/l)	368.7	452.2	446.1
Calculated energy density (Wh/kg)	159.3	211.0	222.0

Table 19. Cell component LFP vs Graphite.

Component LFP vs Graphite	Power optimsed	Mid optimsed	Energy optimsed
Positive electrode area (m^2)	8.5	3.3	1.9
Positive electrode current collector area (m^2)	4.3	1.7	1.0
Positive electrode thickness (µm)	30.3	90.9	151.5
Positive electrode volume fraction	0.6	0.6	0.6
Positive electrode current collector (foil) (µm)	12.0	12.0	12.0
Positive electrolyte volume fraction	0.4	0.4	0.4
Positive electrode additive volume faction	0.1	0.1	0.1
Positive particle diameter (µm)	10.0	10.0	10.0
Negative electrode area (m^2)	9.2	3.7	2.3
Negative electrode current collector area (m^2)	4.6	1.9	1.1
Negative electrode thickness (µm)	25.3	75.9	126.6
Negative electrode volume fraction	0.6	0.6	0.6
Negative electrode current collector (foil) (µm)	10.0	10.0	10.0
Negative electrolyte volume fraction	0.4	0.4	0.4
Negative electrode additive volume fraction	0.0	0.0	0.0
Negative particle diameter (µm)	10.0	10.0	10.0
Separator thickness (µm)	16.0	16.0	16.0
Separator porosity	0.4	0.4	0.4
Areal capacity (mA/cm^2)	1.0	3.0	5.0
Simulated capacity 3.65-2.5 V (Ah) @0.1C	81.0	94.5	90.5
Simulated energy 3.65-2.5 V (Wh) @0.1C	266.3	310.5	296.8
Calculated Cell capacity (Ah)	85.4	99.7	95.5
Calculated Cell energy (Wh)	281.9	329.0	315.1
Calculated energy density (Wh/l)	285.8	333.5	319.4
Calculated energy density (Wh/kg)	134.4	175.0	181.7